Journal Pre-proofs

Glial cell activation and altered metabolic profile in the spinal-trigeminal axis in a rat model of multiple sclerosis associated with the development of trigeminal sensitization

Giulia Magni, Silvia Pedretti, Matteo Audano, Donatella Caruso, Nico Mitro, Stefania Ceruti

PII: S0889-1591(20)30385-8
DOI: https://doi.org/10.1016/j.bbi.2020.07.001
Reference: YBRBI 4212

To appear in: *Brain, Behavior, and Immunity*

Received Date: 22 March 2020
Revised Date: 19 June 2020
Accepted Date: 3 July 2020

Please cite this article as: Magni, G., Pedretti, S., Audano, M., Caruso, D., Mitro, N., Ceruti, S., Glial cell activation and altered metabolic profile in the spinal-trigeminal axis in a rat model of multiple sclerosis associated with the development of trigeminal sensitization, *Brain, Behavior, and Immunity* (2020), doi: https://doi.org/10.1016/j.bbi.2020.07.001

Full-length research report

Glial cell activation and altered metabolic profile in the spinal-trigeminal axis in a rat model of multiple sclerosis associated with the development of trigeminal sensitization

Giulia Magni, Silvia Pedretti, Matteo Audano, Donatella Caruso, Nico Mitro, Stefania Ceruti

Department of Pharmacological and Biomolecular Sciences –
Università degli Studi di Milano –Milan (Italy)

Word count (excluding references, tables and figure legends): 6684

Author for correspondence:
Stefania Ceruti, PhD
Department of Pharmacological and Biomolecular Sciences – Università degli Studi di Milano
via Balzaretti, 9 -20133 Milan (Italy)
Tel.: +39-0250318261
Fax: +39-0250318284
Email address: stefania.ceruti@unimi.it

Abstract

Trigeminal neuralgia is often an early symptom of multiple sclerosis (MS), and it generally does not correlate with the severity of the disease. Thus, whether it is triggered simply by demyelination in specific central nervous system areas is currently questioned. Our aims were to monitor the development of spontaneous trigeminal pain in an animal model of MS, and to analyze: i) glial cells, namely astrocytes and microglia in the central nervous system and satellite glial cells in the trigeminal ganglion, and ii) metabolic changes in the trigeminal system. The subcutaneous injection of recombinant MOG_{1-125} protein fragment to Dark Agouti male rats led to the development of relapsing-remitting EAE, with a first peak after 13 days, a remission stage from day 16 and a second peak from day 21. Interestingly, orofacial allodynia developed from day 1 post injection, i.e. well before the onset of EAE, and worsened over time, irrespective of the disease phase. Activation of glial cells both in the trigeminal ganglia and in the brainstem, with no signs of demyelination in the latter tissue, was observed along with metabolic alterations in the trigeminal ganglion. Our data show, for the first time, the spontaneous development of trigeminal sensitization before the onset of relapsing-remitting EAE in rats. Additionally, pain is maintained elevated during all stages of the disease, suggesting the existence of parallel mechanisms controlling motor symptoms and orofacial pain, likely involving glial cell activation and metabolic alterations which can contribute to trigger the sensitization of sensory neurons.

Keywords: trigeminal pain; astrocytes; microglia; satellite glial cells; metabolomics; experimental autoimmune encephalomyelitis

1. Introduction

Pain is a highly disabling symptom of multiple sclerosis (MS), with an estimate incidence of up to 75% of patients at any disease stage [6]. Trigeminal (TG) neuralgia is one of the worst MS-associated neuropathic pain syndromes, with a 20-fold higher risk in patients than in the general population and a prevalence around 4% [19]. While some authors reported a correlation between TG neuralgia and TG nerve lesions and demyelinating plaques in the pons and in the brainstem [47], other studies found no direct relationship [14]. Retrospective analyses also showed that TG pain is often an early or even an onset symptom of MS, which does not generally correlate with the severity of the disease [34]. Thus, epidemiological data suggest that pain and clinical signs in MS are triggered by parallel but independent yet-to-be identified mechanisms.

The role of the so-called “neuroimmune interface”, consisting of central nervous system (CNS) microglia, astrocytes, oligodendrocytes, and of infiltrating T cells and macrophages, in modulating the excitability of neurons in pain pathways and in the transition from acute to chronic pain is now clearly established [15]. Spinal cord microglia sense painful stimuli from the periphery and react by changing shape and releasing bioactive factors (e.g., cytokines, growth factors, ATP) which not only sensitize second-order neurons but can also promote reactive astrogliosis [23]. Reactive astrocytes, in turn, further sustain microglia reaction and modulate neuronal firing leading to a complex cross-talk that promotes pain development and chronicization [42]. Additionally, in sensory ganglia neuronal bodies are surrounded and wrapped by satellite glial cells (SCGs) [51], which become activated after inflammation and nerve damage and together with infiltrating macrophages and immune cells contribute to neuronal sensitization [33;46]. Also alterations of fatty acid metabolism negatively impact the homeostatic support to neurons exerted by glial cells [4] and can contribute to pain and neurodegeneration [38].

The first paper demonstrating the development of orofacial allodynia at the onset of motor signs of chronic Experimental Autoimmune Encephalomyelitis (EAE) in mice also showed T cell infiltration and glial activation along the TG primary afferent pathway, and demyelination at the TG sensory root and spinal-trigeminal tract. Interestingly, despite orofacial sensitivity, glial cell activation was absent during the chronic phase of the disease, suggesting that compensatory mechanisms take place to bring back cells to their basal state, which cannot hinder pain chronicization [50]. Conversely, other authors described the development of spontaneous TG pain and hind paw hypersensitivity before the onset of EAE in mice but with no signs of astrogliosis/microgliosis up to the chronic phase. They show a slight but significant peripheral

infiltration of CD3+ cells in the TG ganglion and nerve in the preclinical phase [13], along with a specific protective role played by Treg lymphocytes and remyelination of the facial nociceptive pathway [12].

Overall, available data suggest that activation of glial cells can represent one of the key events driving the early development of MS-associated painful states, preceding the appearance of motor signs of the pathology both in clinics and in preclinical models of chronic EAE. To the best of our knowledge, no data are currently available on the spontaneous development of TG sensitization and on its relationship with disease progression in animal models of relapsing-remitting MS, the most common form of the disease in young adults [53]. Our study was aimed at filling this gap.

2. Methods

2.1 Animals

Male Dark Agouti rats weighing about 200 g have been purchased from Envigo (Italy). We chose to use male animals in which a role for glial cells in the development of pain has been consistently demonstrated, whereas conflicting results are available in females [32;17]. We have strictly adhered to the current Italian and European rules on the use of laboratory animals in science; authorizations for the use of animals have been granted by the Italian Ministry of Health (authorization numbers #810/2017-PR; #825/2019-PR). Consistently with Article 13, Paragraph 2 of the 26/2014 Italian Legislative Decree, we have employed procedures that require the minimum number of animals. Moreover, we made all possible efforts to apply the Reduce, Refine and Replace (3Rs) rule to our experiments. Housing of rats and all the procedures on living animals have been conducted by authorized and trained personnel only. Animals were randomly assigned to the different experimental groups, and behavioral measurements including motor scoring and evaluation of TG sensitization were performed by an investigator blinded to group assignments.

2.2 Evaluation of TG sensitization

Animals in the three experimental groups have been subjected to evaluation of orofacial sensitivity. The orofacial skin region, near to the center of the vibrissae pad, has been tested daily up to animal's sacrifice with von Frey filaments of ascending thickness and force, as described [30]. The response threshold was defined as the lowest force required to elicit at least three head withdrawal responses out of five tests, performed within few seconds. A daily 7-days long training

was performed before EAE induction, to get animals acquainted with the operator and with the procedure, and to determine basal head withdrawal threshold value for each animal (Figure 1).

2.3 Induction of EAE and evaluation of associated motor deficits

EAE has been induced via intradermal injection of 8.75 µg of recombinant MOG_{1-125} emulsified in incomplete Freund's adjuvant (IFA) and sodium acetate (25mM, pH 4.0) into the dorsal skin just rostral to the base of the tail, as described in literature [37]. Naïve animals received no treatment, apart from the evaluation of orofacial mechanical allodynia (see 2.2), whereas Control (CTR) rats were injected with IFA and sodium acetate only. From day post immunization (DPI) 1, rats were monitored daily for signs of neurological motor deficits according to the following scale: 0, absence of symptoms; 1, partial tail paralysis; 2, full tail paralysis; 3, hindlimb weakness (unsteady gait while walking); 4, partial hindlimb paralysis (no weight bearing but observable movement of the limb); 5, full hindlimb paralysis; 6, complete paralysis of lower body (rat is unable to hold his belly up from the ground); 7, euthanasia due to disease progression [37]. We never observed scores of 6 or 7 in this study. If difficulties in reaching water and food were observed, they were located on the bottom of the cage. The onset of EAE (i.e. the day on which a rat shows first signs of motor impairment, usually score 1) was recorded for each animal, and it was detected between days 8/9 (60% of EAE animals, 24/40) and 11. Only 2/40 animals showed no signs of motor impairment at any time point and were therefore excluded from the experiment. Changes in animals' body weight and the development of orofacial allodynia (see 2.2) were also evaluated daily. At DPI 21, animals were deeply anesthetized with ketamine (90 mg/kg) and xylazine (10 mg/kg) and sacrificed depending to the subsequent analyses to be performed (i.e., by decapitation for Western blotting, Real-time PCR and metabolomics analyses or by transacardial perfusion with PBS followed by 4% formalin and decapitation for immunohistochemical analyses) [30].

2.4 Myelin staining

To mark myelin integrity, Fluoromyelin red staining was also performed, as described [9]. In detail, brainstem sections were acclimatized at room temperature for 10 min, rinsed three times with PBS 1x and incubated for 20 min RT with Fluoromyelin red (1:150 in PBS 1x; Thermofisher Scientific, Milan, Italy). After being rinsed three times with PBS 1x, slides were mounted with Dako Fluorescence Mounting Medium (Dako, Denmark). Images of brainstem sections were collected at low (10X) magnification thanks to the Hamamatsu NanoZoomer S60 slide scanner, converted to

grayscale and subjected to densitometric analysis. The mean value of pixel intensity was evaluated by the NIH Image-J software [40], and expressed as integrated density compared to values obtained in Naïve animals set to 1.

2.5 Immunohistochemistry and image analysis

After sacrifice, the TG ganglia and brainstems were excised, postfixed in 4% formalin for 60–90 min, cryoprotected in 30% sucrose (48 h), embedded in mounting medium (OCT; Tissue Tek, Sakura Finetek, Zoeterwoude, Netherlands), and cut longitudinally on a cryostat at 20 µm thickness. Brainstems were cut at the level of the medulla oblongata [51]. TGs from each animal were embedded together. Sections were incubated for 45 min in PBS containing 10% normal goat serum (Sigma-Aldrich, Merck group) and 0.1% Triton X-100 (Sigma–Aldrich, Merck group), and then overnight at RT with the following primary antibodies: rabbit antibodies against the microglia marker ionized calcium binding adaptor molecule 1 (anti-Iba1, 1:500; Wako, Richmond, VA, USA) or the astrocyte/satellite glial cell marker glial fibrillary acidic protein (anti-GFAP, 1:600; Dako, Milan, Italy), and mouse antibodies against the neuronal nuclei marker (anti-NeuN, 1:150; Chemicon, Vimodrone, Italy). Sections were then rinsed three times with PBS and incubated for 1 h RT with the AlexaFluor® 488- or AlexaFluor® 555-conjugated secondary antibodies (1:600; Life Technologies, Milan, Italy). All antibodies were diluted in PBS containing 0.1% Triton X-100 and 5% normal goat serum. Cell nuclei were counterstained with the Hoechst33258 dye (1:20,000; Sigma-Aldrich, Merck group). Samples were finally examined with a laser scanning confocal microscope (LSM 510, Zeiss, Milan, Italy), and images were acquired and processed using the LSM Image Browser software (Zeiss).

2.5.1 Cell counting

The number of Iba1+ cells (TG, brainstem) and the number of GFAP-encircled neurons (TG) were counted in whole TG or brainstem sections acquired at 20X magnification and expressed as number of positive cells/area (see Figure legends for details).

2.5.2 Densitometric analysis of GFAP staining

A digital image of the brainstem immunostained sections was acquired at low (10X) magnification thanks to the Hamamatsu NanoZoomer S60 slide scanner, converted to grayscale and the mean values of pixel intensity were automatically evaluated using the NIH Image-J software

[27;40], and expressed as integrated density compared to values obtained in Naïve animals set to 1.

Discrete areas of the same sections showing signs of cell hypertrophy were acquired at 20X magnification and converted to binary grayscale for analysis (not shown). The average cell size and the % area stained with GFAP were evaluated by the ‘‘Particle analysis’’ tool of the Fiji-ImageJ software [39]. Data are expressed as fold over values obtained in Naïve animals set to 1.

2.5.3 Evaluation of microglia morphology and branch complexity

Iba1-immunostained brainstem sections were acquired at 20X magnification and converted to binary grayscale to better analyze microglial cell morphology (Figure 4). The average cell size and the integrated optical density were evaluated by the ‘‘Particle analysis’’ tool of the Fiji-ImageJ software [29;39]. Data are expressed as fold over values obtained in Naïve animals set to 1.

2.6 Western blotting

Western blotting analysis of brainstem tissues was performed, as described before [30]. Mouse antibodies directed against: i) GFAP (1:1,000; Cell Signaling, Danvers, MA, USA), or ii) the marker of mature oligodendrocyte 2’,3’-cyclic-nucleotide 3’-phosphodiesterase (CNPase, 1:250; Millipore, Vimodrone, MI, Italy) and rat antibody against myelin basic protein (MBP, 1:500; Millipore) as markers of myelinating oligodendrocytes, were used. Alpha-tubulin (mouse anti α-tubulin, 1:1,000; Sigma-Aldrich) expression was analyzed as internal loading control. Next, filters were incubated with species-specific secondary antibodies conjugated to horseradish peroxidase (goat anti-rabbit, 1:4,000 and goat anti-mouse, 1:2,000; both from Sigma-Aldrich; goat anti-rat, 1:2,000; Thermo Fisher Scientific). Protein detection was performed by ECL (BioRad, Milan, Italy). After autoradiography, the relative amount of protein was evaluated by the NIH Image-J software, normalized for the corresponding α-tubulin values, and expressed with respect to values obtained in Naïve animals set to 1. In the case of GFAP and MBP, multiple specific protein bands were analyzed altogether.

2.7 Real-time PCR

Total RNA was extracted from brainstem tissues using Trizol reagent (Life Technologies, Monza, Italy). cDNA synthesis was performed starting from 800 ng of total RNA using SuperScript II Reverse Transcriptase (Life Technologies), as described [9]. The expression of all genes was analyzed

using Sybr-green reagents (Bio-Rad, Milan, Italy) and normalized to GAPDH expression using CFX96 real-time PCR system (Bio-Rad) following the manufacturer's protocol. The Ct values were elaborated with the comparative CT method (ΔΔCT) which allows the relative quantification of template comparing the expression levels of the interested gene with the ones of the housekeeping gene. Primer sequences are reported in Table 1.

Table 1. List of primers for Real-time PCR utilized in this study

Gene	Primer sequence (5'-3')
A_3AR-fw	GCACTCTTGGATTTGGCTGC
A_3AR-rv	GTAGACCTCAGCCACTTAGCC
GFAP-fw	GGTGTGGAGTGCCTTCGTATT
GFAP-rv	GGGACACTTTCAGCTCCATTTC
Iba1-fw	CTCATCGTCATCTCCCCACC
Iba1-rv	ACCTCTCTTCCTGTTGGGCT
IL1β-fw	TGGCAACTGTCCCTGAACTC
IL1β-rv	GTCGAGATGCTGCTGTGAGA
P2X4-fw	AAGGTGTGGCTGTGACCAAC
P2X4-rv	AGGAATCTCTGGACAGGTGC
$P2Y_{12}$-fw	CTCACCAACAGGAGGCCAAA
$P2Y_{12}$-rv	GTGCCAGACCAGACCAAACT
S1P1-fw	TTCAGCCTCCTTGCTATCGC
S1P1-rv	AGGATGAGGGAGATGACCCAG

fw: forward; rv: reverse

2.8 Metabolomic analyses of trigeminal ganglia and nerves

After animals' sacrifice, TG ganglia and nerves (the anterior portion from the facial bones up to the ganglion and the afferent portion projecting from the ganglion to the brainstem) were rapidly excised, snap frozen in dry ice, and stored at -80°C up to the analysis. TG ganglia and nerves were then resuspended in 250µl methanol/acetonitrile 1:1 containing [U-$^{13}C_6$]-Glucose (Sigma Aldrich, 389374), [U-$^{13}C_5$]-Glutamine (Sigma Aldrich, 605166), [U-$^{13}C_{16}$]-palmitic acid (Sigma Aldrich, 605573) 1ng/µl as internal standards, lysed by TissueLyser at the highest frequency and then spun at 20,000g

for 5 min at 4°C. Supernatants were then passed through a regenerated cellulose filter, dried and resuspended in 100µl of MeOH for subsequent analysis. Amino acids quantification was performed through previous derivatization. Briefly, 50µl of 5% phenyl isothiocyanate (PITC) in 31.5% EtOH and 31.5% pyridine in water were added to 10µl of each sample. Mixtures were then incubated with PITC solution for 20 min at RT, dried under N_2 flow and suspended in 100µl of 5mM ammonium acetate in MeOH/H_2O 1:1. Metabolomic data were performed on an API-4000 triple quadrupole mass spectrometer (AB Sciex) coupled with a HPLC system (Agilent). The identity of all metabolites was confirmed using pure standards. Quantification of different metabolites was performed with a liquid chromatography/tandem mass spectrometry (LC-MS/MS) method using a C18 column (Biocrates) for amino acids and cyano-phase LUNA column (50mm x 4.6mm, 5µm; Phenomenex) for energetic metabolites, respectively. Methanolic samples were analyzed by a 10 min and 3 min run in positive (amino acids) and 5 min run in negative (all other metabolites) ion mode with a 21 multiple reaction monitoring (MRM) transitions in positive ion mode and 30 MRM transitions in negative ion mode, respectively. The mobile phases for positive ion mode analysis (amino acids) were as follows: phase A, 0.2% formic acid in water and phase B, 0.2% formic acid in acetonitrile. The gradient was T_0 100%A, $T_{5.5min.}$ 5%A, T_{7min} 100%A with a flow rate of 500µl/min. The mobile phases for negative ion mode analysis (all other metabolites) were as follows: phase A, Water and B, 2 mM ammonium acetate in MeOH. The gradient was 90% B for all the analysis with a flow rate of 500µl/min.

Phospholipids were evaluated by LC-MS/MS according to published protocol [5] with some modifications, as follows. The same methanolic extracts described above were analyzed by LC-MS/MS using XTerra Reverse Phase C18 column (3.5 µm 4,6x100mm, Waters) and MeOH with 0.1% formic acid as isocratic mobile phase with 274 multiples reaction monitoring (MRM) transitions for positive ion mode in 5 minutes total run for each sample. LC-ESI-MS/MS for negative ion mode was conducted with a cyano-phase LUNA column (50mm x 4.6mm, 5µm; Phenomenex) and 5mM ammonium acetate pH 7 in MeOH as isocratic mobile phase with 50 MRM transitions in 5 minutes total run for each sample. The identity of the different phospholipid families was confirmed using pure standards, namely one for each family. An ESI source connected with an API 4000 triple quadrupole instrument (AB Sciex, USA) was used. For all the analyses described MultiQuant™ software (version 3.0.2) was used for data analysis and peak review of chromatograms.

Metabolomic data were normalized as previously described [1] by defining x_n^N (relative metabolite area) as:

$$x_n^N = \frac{Xn}{\sum_{n=a}^{z} n}$$

where x_n represents the peak areas of metabolite *n* for samples *a, b,…, z* and $\sum_{n=a}^{z} n$ represents the sum of peak areas of metabolite *n* for samples *a, b,…, z.*

Relative metabolite area (x_n^N) was then divided by the sum of relative metabolite areas analyzed in each sample to obtain relative metabolite abundance (*m*), as:

$$m_a^N = \frac{x_n^N}{\sum_{a=1}^{n} a}$$

where $\sum_{a=1}^{n} a$ represents the sum of relative metabolite areas *1, 2, …, n* for sample *a.* Internal standards were used to control instrument sensitivity.

2.9 Statistical analysis

Data are presented as mean±SEM and have been analyzed with the GraphPad Prism 7.0 software. For all comparisons between two groups with a normal distribution, two-tailed unpaired Student t-test was performed. For multiple comparison testing, one- or two-way analysis of variance (ANOVA) accompanied by Tukey's post-hoc test was used. Differences were considered significant for $P<0.05$. Correlation analysis between the gene expression of the glial markers Iba1/GFAP and purinergic receptors or IL-1β was performed by applying the Pearson's correlation test; $P<0.05$ was considered as statistically significant correlation.

Metabolic data were analyzed using Metabonalyst software (www.https://www.metaboanalyst.ca/) [8]. One-Way ANOVA was performed using Fisher's post-hoc test with low standard deviation to report only significant affected metabolites commonly changed in both comparisons analyzed: Naïve vs EAE and CTR vs EAE.

3. Results

3.1 Orofacial allodynia precedes the motor signs of EAE and is maintained irrespective of the disease stage

We first set up the model of relapsing-remitting EAE in male Dark Agouti rats, and monitored the possible development of orofacial allodynia in parallel with the motor signs of the pathology. To evaluate orofacial allodynia all rats were subjected to 7-day training to von Frey hairs before the assignment to different experimental groups. As shown in Figure 1 (training), no differences in head withdrawal threshold were detected among animals. Rats were then randomly divided in the three experimental groups: Naïve, no treatment; Control (CTR) injected with IFA and 25mM sodium acetate; EAE injected with 8.75 µg of recombinant MOG_{1-125} emulsified in incomplete IFA and 25mM

sodium acetate. Injection of the MOG_{1-125} peptide led to the first appearance of motor deficits (typically weakness of the tail, score 1) at around DPI 8/9 in the 60% of animals (24/40; Figure 1, black dashed line). We observed an overall typical relapsing-remitting trend of the motor signs of the disease, with a first peak at DPI 13 (mean motor score: 4.19±0.25), followed by a partial remission (DPI 16; mean motor score: 2.14±0.25) and a second peak at DPI 21, when the experiment was ended. No motor impairment was observed in animals belonging to either the Naïve or the CTR group. To the most of our surprise, we observed that EAE animals displayed significant orofacial allodynia, as demonstrated by a progressive decrease in the head withdrawal threshold from DPI 1 (Figure 1, red line), thus preceding the signs of motor impairment detected from DPI 8/9 (Figure 1). Interestingly, orofacial sensitivity progressively worsened over time independently from the stage of the pathology, as shown by the decreased head withdrawal threshold even during the remission phase (DPI 13-17; Figure 1, red line). In line with literature, we also found that development and progression of EAE was accompanied by significant reduction in animals' body weight, starting from DPI 11 and progressively increasing over time (Supplementary figure 1). This is possibly due to the loss of muscle mass and to difficulties in feeding properly [57].

Notably, from DPI 1 a small but significant reduction in the head withdrawal threshold, which remained virtually unmodified over time, was also observed in CTR animals (Figure 1, green line) and was accompanied by the development of unspecific swelling of hind paws at DPI 13 in 16/24 animals. CTR animals were injected with the vehicle of MOG_{1-125} (i.e., IFA + sodium acetate), but paw swelling was never observed in the EAE group. To the best of our knowledge, the present work is the first reporting the comparison among CTR group with Naïve and EAE, and the swelling of hind paws detected in CTR rats may be due to an unspecific inflammatory reaction which rendered animals more sensitive to the Von Frey assay. Nevertheless, the head withdrawal threshold of EAE animals was statistically different also from CTR animals starting from DPI 6 (Figure 1), thus implying that induction of the pathology is adding specific pathogenic mechanisms leading to trigeminal sensitization (see also below). According to the development of unspecific inflammatory response, we also observed a transient reduction of body weight in CTR compared to Naïve animals starting from DPI 15 and normalizing at DPI 19 (Supplementary Figure 1).

Overall, these data suggest that at least two timely-defined and independent pathogenic mechanisms occur in EAE rats: the first driving the development of orofacial allodynia and the second accounting for motor deficits.

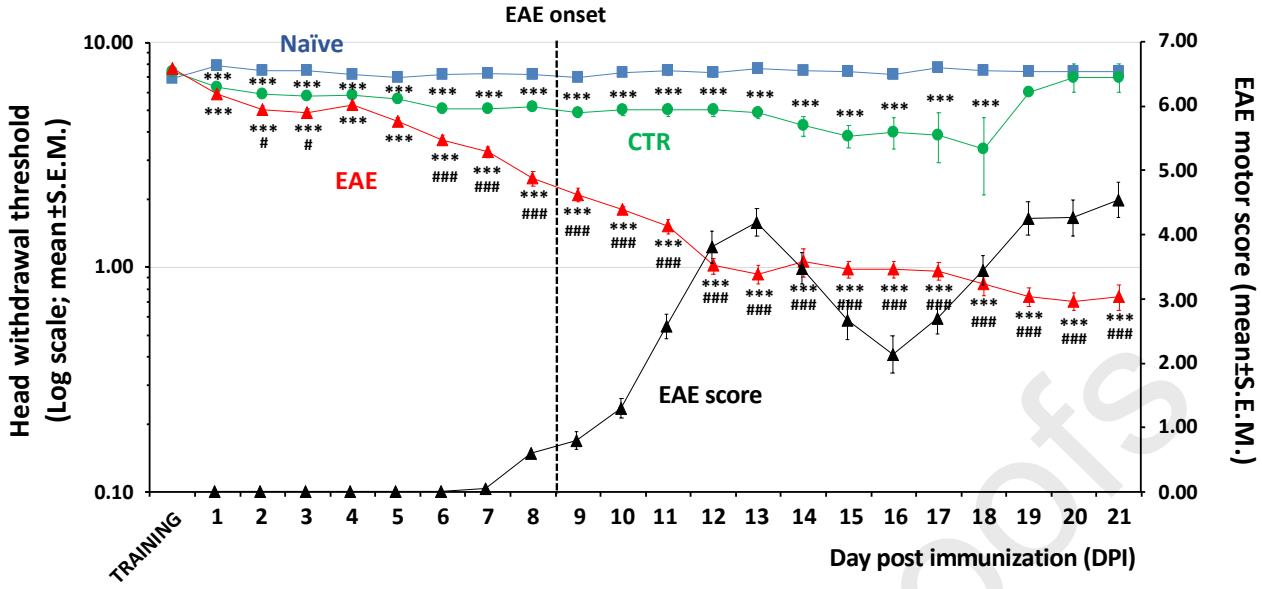

Figure 1. Orofacial mechanical allodynia precedes the appearance of clinical signs of EAE and is maintained independently of the disease stage. *Blue, red and green lines represent the changes in the mean head withdrawal threshold over time in Naïve, CTR and EAE rats, respectively (left Y-axis, Log scale). Black line represents the development of motor signs of EAE, showing a typical relapsing/remitting trend (right Y-axis) [37]. The vertical dotted line highlights the mean day of EAE disease onset (i.e., days 8/9). DPI=day post immunization. N=24 (Naïve; CTR) and N=40 (EAE) rats from 7 independent experiments. ***P<0.001 vs Naïve; #P<0.05, ###P<0.001 vs CTR; two-way ANOVA, Tukey post-hoc test.*

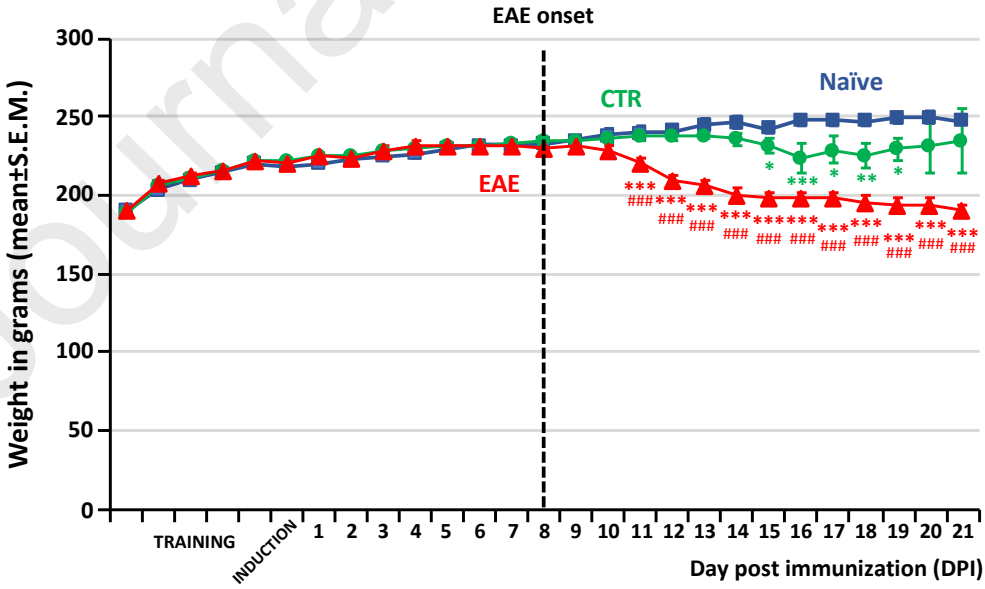

Supplementary figure 1. The development of the clinical signs of EAE is accompanied by progressive loss of animals' weight. *Blue, green and red lines represent the changes over time in animals' weight in Naïve, CTR and EAE rats, respectively. The vertical dotted line highlights the mean*

*day of EAE onset (see Figure 1). From DPI 15, i.e. in parallel with the development of unspecific paw swelling (see text for details), a limited but significant weight loss is observed also in CTR animals. DPI=Day Post Induction. N=24 (Naïve; CTR) and N=40 (EAE) rats from 7 independent experiments. *P<0.05, **P<0.01, ***P<0.001 vs Naïve; ###P<0.001 vs CTR; Two-way ANOVA, Tukey post-hoc test.*

3.2 Myelin structure is not modified in the brainstem of EAE animals

To verify whether orofacial sensitization was linked to EAE-induced demyelination in the first station of the central nervous system (CNS) receiving trigeminal projections, i.e. the brainstem [51], we performed both Western blotting analysis of markers of mature myelinating oligodendrocytes and staining of myelin by Fluoromyelin red dye. No differences in either CNPase or MBP protein expression were observed (Figure 2A) as well as in Fluoromyelin staining (Figure 2B) in the brainstem of animals from the three experimental groups at DPI 21, suggesting that myelin alterations are not involved in the development of trigeminal sensitization.

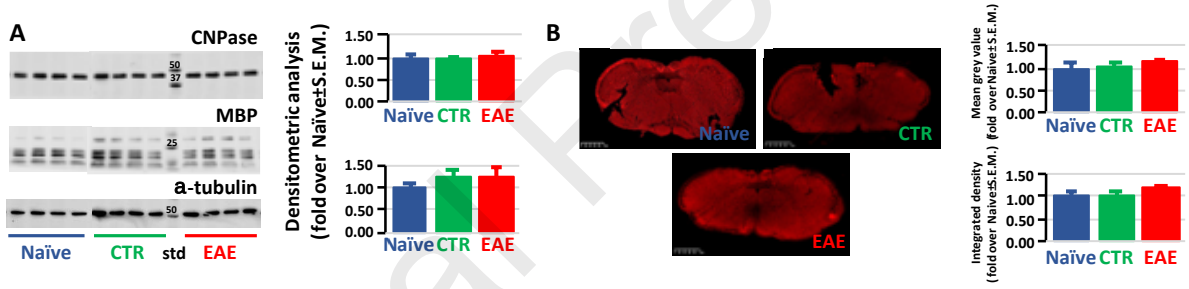

Figure 2. No changes in the expression of myelin proteins in the brainstem of EAE animals at DPI 21. A, left: *representative Western blotting analysis of CNPase and MBP proteins performed on the same nitrocellulose filter cut in two parts. Each line represents 1 animal. Multiple bands were detected for MBP, which have been analyzed altogether. The upper part of the filter was then stripped, and immunostaining for α-tubulin performed as internal control. The apparent molecular weight of standard proteins (std) is indicated.* ***Right:*** *densitometric analysis of protein expression. Each value has been normalized on the corresponding α-tubulin content and expressed as fold over the mean value in the Naïve group. N=5 (Naïve), N=6 (CTR) and N=13 (EAE) rats from 3 independent experiments.* ***B, left:*** *representative Fluoromyelin red myelin staining of brainstem sections. Scale bars: 1 mm.* ***Right:*** *Images have been converted to grayscale and the densitometric analysis of staining intensity performed by the ImageJ software. Results show no differences among the 3 experimental groups. N=3 (Naïve, CTR), and N=4 (EAE) sections from independent animals.*

3.3 Reactive astrogliosis and microgliosis in the brainstem of EAE animals at DPI 21

We next evaluated the activation of glial cells, i.e. astrocytes and microglia, in the brainstem of animals from the three groups at DPI 21. Concerning astrocytes, real-time PCR showed a 2.5-fold increase in the expression of GFAP in EAE animals compared to both Naïve and CTR groups (Figure 3A). This result was further confirmed by Western blotting analysis (Figure 3B). Conversely, densitometric analysis of immunostained sections showed no significant differences among the three groups when brainstem sections were considered as a whole at low magnification (Figure 3C). However, discrete tissue areas with typical signs of reactive astrogliosis (i.e., with hypertrophic and intensely stained cells) were detected at higher magnification in the brainstem of EAE animals only (Figure 3D). Analysis of GFAP staining intensity and of cell morphology in these portions of the tissue by the FIJI Image J software (see Methods) showed an increase in the % of stained area and of the average size of GFAP-positive cells in EAE animals with respect to both Naïve and CTR groups (Figure 3D, histograms), thus confirming the development of reactive astrogliosis.

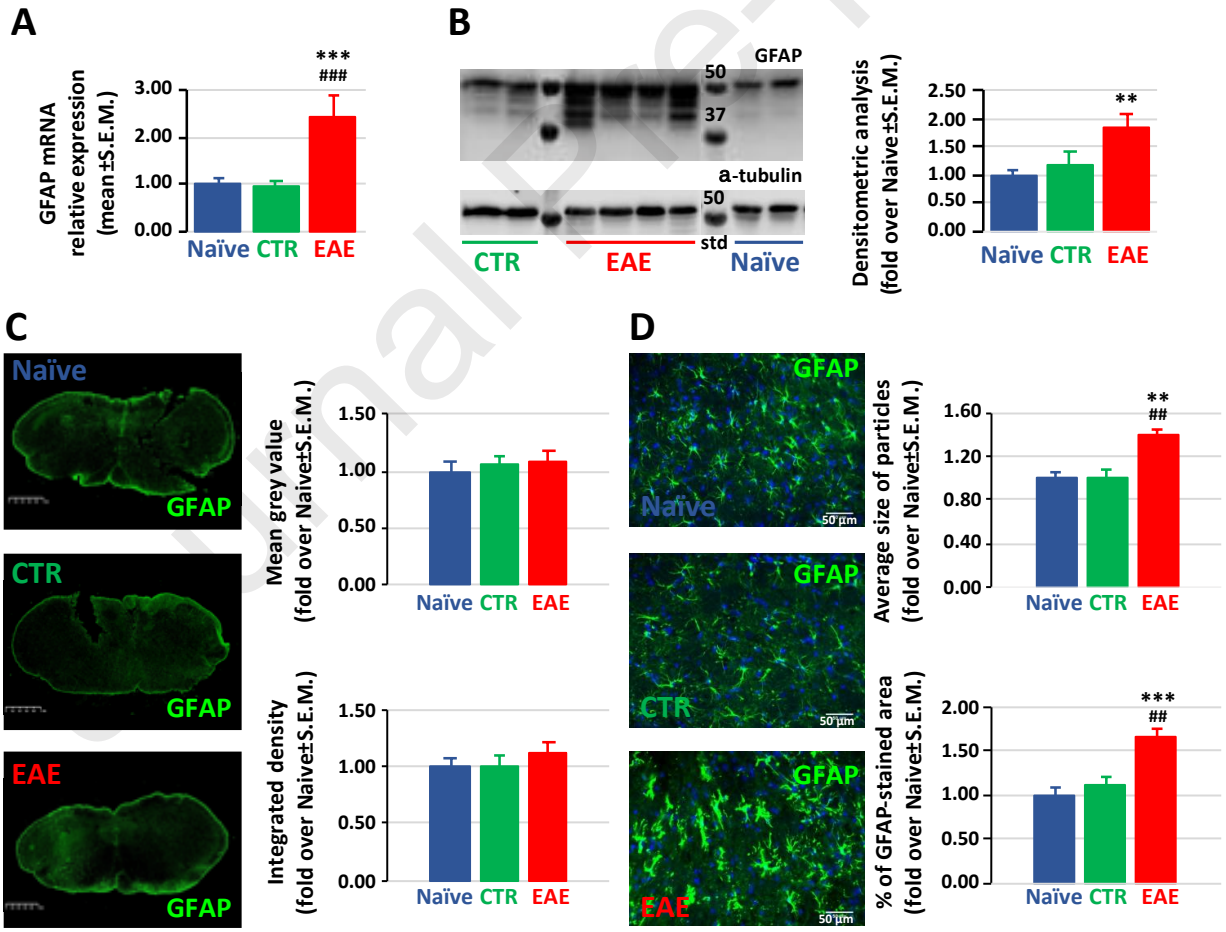

Figure 3. Signs of reactive astrogliosis in the brainstem of EAE animals at DPI 21. A: *Real-time qPCR evaluation of GFAP mRNA expression in the brainstem of animals in each experimental group. N=10 animals/condition from 4 independent experiments.* ***B:*** *representative Western blotting analysis of*

GFAP expression in the brainstem of rats at DPI 21. Several protein bands are detected between 50 and 37 KDa, as expected [30], which have been analyzed altogether for each sample, normalized for the corresponding α-tubulin content, and expressed as fold over Naïve values. N=8 (Naïve, EAE) and 3 (CTR) rats from 2 independent experiments. ***C:*** *representative images of brainstem sections after IHC staining for GFAP. Images have been converted to grayscale and the densitometric analysis of staining intensity performed by means of the ImageJ software. No differences have been detected among experimental groups (histograms). Scale bars: 1 mm.* ***D:*** *magnifications of portions of the sections in C, showing signs of reactive astrogliosis and astrocyte hypertrophy in discrete areas of EAE brain tissue. Images have been converted to black and white and the "particle analysis" Fiji/ImageJ tool was utilized on black and white images to measure the average size of GFAP-positive particles and the % of the total area analyzed showing GFAP staining (histograms). Scale bars: 50 μm. N=6 sections from 4 animals/group. **P<0.01, ***P<0.001 vs Naïve; ##P<0.01, ###P<0.001 vs CTR; one-way ANOVA, Tukey post-hoc test.*

Evaluation of the expression of the microglial marker Iba1 showed a highly significant upregulation in the brainstem of EAE animals compared to the other two groups, both at the RNA and protein level (Figure 4A,B). Distinctly from astrogliosis, microgliosis was already evident at low magnification in brainstem sections immunostained with a specific antibody (Figure 4C, left column). Higher magnification images clearly showed an increased number of Iba1-positive cells in the EAE group (Figure 4C, center column), as quantified in histograms in Figure 4D (more than 5-fold increase in EAE with respect to Naïve and CTR animals). To better highlight the morphological signs of activated microglia, we acquired the whole sections at higher magnification, converted images to grayscale (Figure 4C, right column) and applied the Particle analysis of the FIJI Image J software (see Methods). Results show a 3-fold increase in the Iba1-stained area (Figure 4E) and a more than 2-fold increase in the average size of microglia cells (Figure 4F) in the EAE group. Overall, these data suggest that development of EAE has led to the appearance of an increased number of bigger and highly stained microglia cells, which could be responsible, along with reactive astrocytes, of the development of orofacial allodynia. Interestingly, a significant correlation between Iba1 and GFAP expression data by real-time PCR was found in the EAE group (R^2=0.7846, P=0.0006) with respect to Naïve (R^2=0.1099, P=0.3493) animals, suggesting parallel EAE-induced reactive astrogliosis and microgliosis in the brainstem at least at later DPIs. A weak positive correlation is

observed in the CTR group (R^2=0.4499, P=0.0337), but with extremely low values for both GFAP and Iba1 expression (see green dots on the X-axis in graphs in Figure 5).

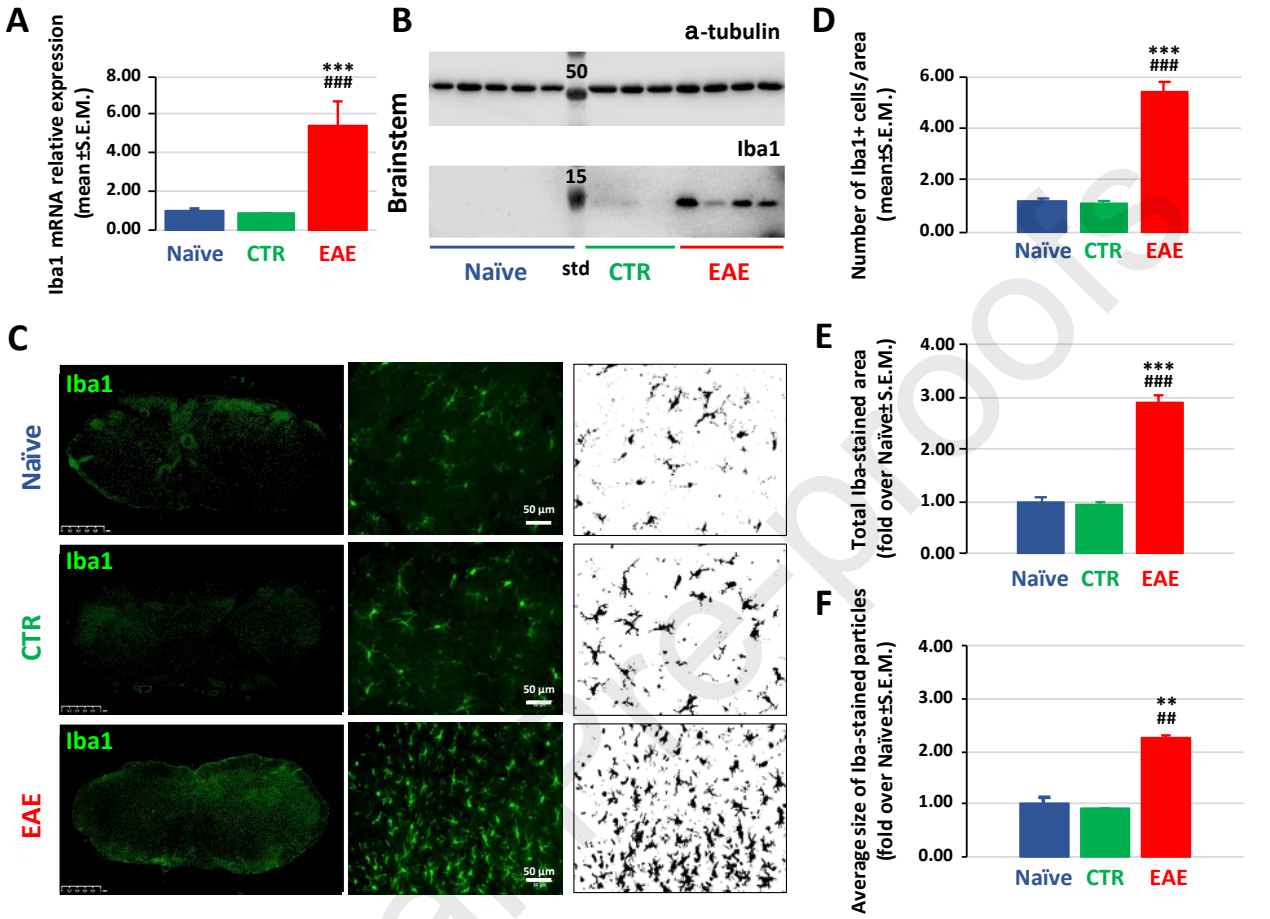

Figure 4. Activation of microglia in the brainstem of EAE animals at DPI 21. A: *Real-time qPCR showing mRNA expression of the microglia marker Iba1. N=10 animals/condition.* ***B:*** *representative Western blotting filters showing Iba1 protein expression in the brainstem of EAE rats at DPI 21, and lack of expression in Naïve and CTR groups. α-tubulin expression was evaluated as protein loading control.* ***C, left:*** *representative images of brainstem sections in each experimental condition after IHC staining for Iba1. Scale bars: 1 mm. Middle: magnification of representative section areas. Scale bars=50 µm.* ***Right:*** *images converted to black and white to reduce background noise.* ***D:*** *number of Iba1-positive cells counted in 6 sections from 4 animals/condition. The "particle analysis" Fiji/ImageJ tool was utilized on black and white images to measure the total Iba1-stained area in the whole section (**E**) and the average size of Iba1-positive particles (**F**). N=6 sections from 4 animals/condition. **P<0.01, ***P<0.001 vs Naïve; ##P<0.01, ###P<0.001 vs CTR; one-way ANOVA, Tukey post-hoc test.*

3.4 Increased expression of IL-1β and of glial purinergic receptors in the brainstem of EAE animals at DPI 21

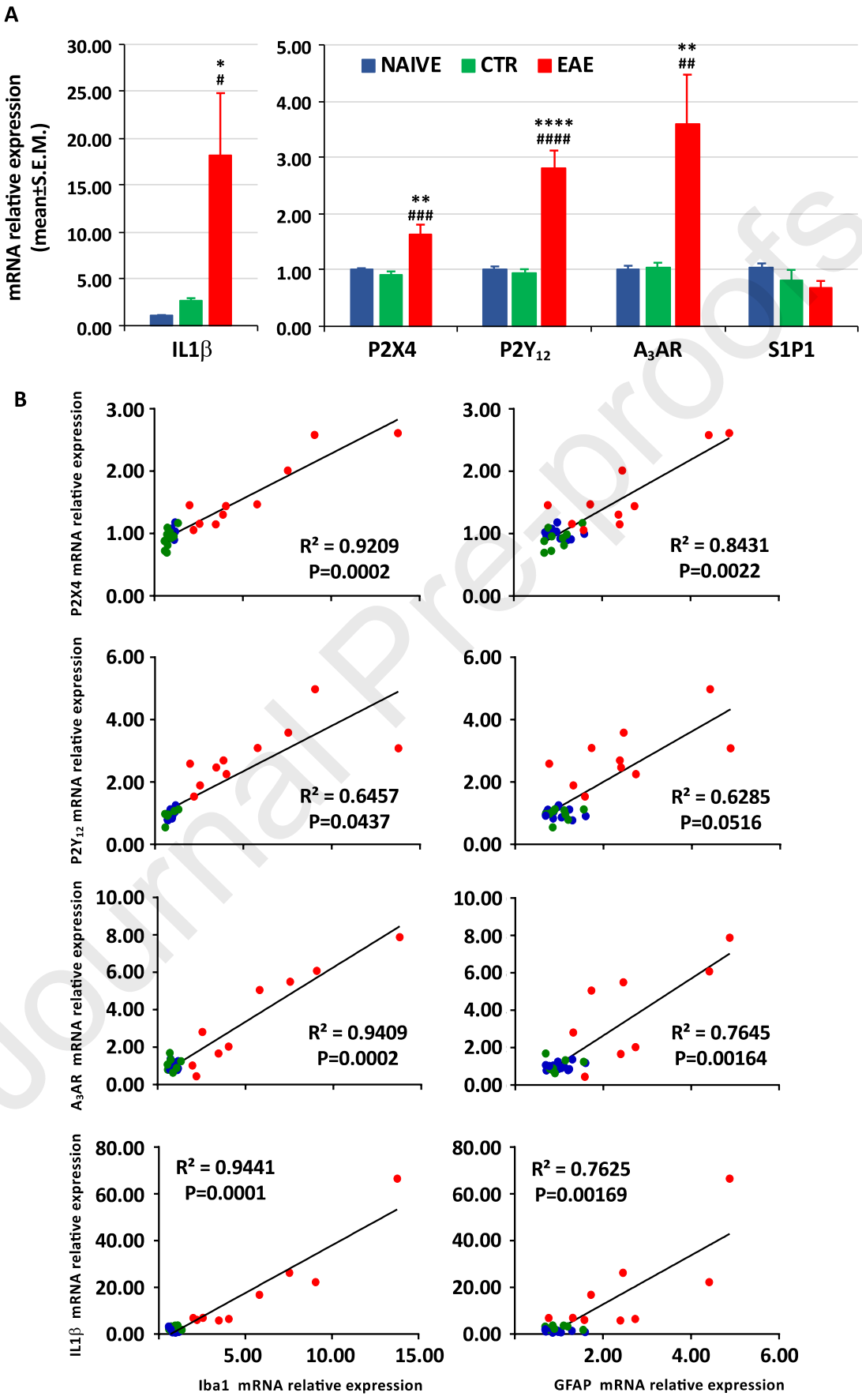

Figure 5. Increased expression of glial purinergic receptors and of IL-1β in the brainstem of EAE animals at DPI 21. A: *Real-time qPCR showing mRNA expression of IL-1β and of the P2X4 and $P2Y_{12}$ nucleotide receptors, of the A_3 adenosine receptor, and of the sphingosine-1-phosphate receptor 1 (S1P1) in the brainstem of Naïve, CTR and EAE animals at DPI 21.* ***B:*** *Pearson correlation between the expression of the glial markers Iba1 or GFAP (X axis) and of the various purinergic receptors or IL-1β. The R^2 and P values refer to EAE samples. N=8 (Naïve), 9 (CTR) and 10 (EAE) animals from 4 independent experiments. *P<0.05, **P<0.01, ****P<0.0001 vs Naïve; #P<0.05, ##P<0.01, ####P<0.0001 vs CTR; one-way ANOVA, Tukey post-hoc test.*

After EAE induction, glial cell activation in the brainstem was accompanied by signs of inflammation, as demonstrated by a 18-fold increase in the expression of IL-1β mRNA (Figure 5A). We also evaluated the mRNA expression of selected nucleotide and nucleoside purinergic receptors, based on their key role in the modulation of the functions of astrocytes and microglia, and on their involvement in pain transmission [28]. Real-time PCR data showed a significant upregulation of the expression of the ionotropic P2X4 and of the metabotropic $P2Y_{12}$ nucleotide receptors, and of the metabotropic A_3 adenosine receptor (A_3AR) subtypes (Figure 5A). Pearson correlations between the expression of the selected genes and of either Iba1 or GFAP showed highly significant correlations between Iba1 and P2X4, A_3AR and IL-1β expression in the EAE group (Figure 5B, left graphs). Lower but still significant correlation was instead found between Iba1 and $P2Y_{12}$ receptor and between GFAP expression and the four evaluated genes (Figure 5B). This suggests that the observed changes in the expression of a pro-inflammatory cytokine and of selected purinergic receptors are directly related to EAE-induced glia reactivity and could contribute to sustain TG sensitization.

Since we have performed our analyses at DPI 21, at present we cannot exclude that the observed changes are a consequence rather than a cause of EAE-induced TG sensitization. Thus, we have performed one preliminary experiment in which we have sacrificed animals when they showed the first motor signs of EAE (i.e., EAE onset, around DPI 8-11) in comparison with CTR animals. Real-time PCR analysis showed an already significant upregulation of GFAP and Iba1 along with IL-1β mRNA expression in the brainstems of animals (Supplementary figure 2A), which is confirmed by the presence of two distinct clusters of samples as a function of glial markers when single values are analyzed in a XY correlation plot (Supplementary figure 2B, C). This suggests that glial cell activation is an early event in EAE pathology, and further highlights the importance of an in-depth analysis of the pathways that link glial cell reaction to the development of TG pain to identify possible

pharmacological approaches. Interestingly, neither P2X4 nor $P2Y_{12}$ nucleotide receptors are upregulated at this early time point, while a non-significant trend to upregulation is observed in the case of A_3AR (Supplementary figure 2A), which makes this receptor subtype a possible interesting target for early approaches to the pathology as further supported by the significant correlation observed between A_3AR and Iba1 expression in the EAE group (Supplementary figure 2C). No significant correlations either between Iba1 and GFAP (Supplementary figure 2B) or between glial markers and P2 receptors or IL-1β expression (Supplementary figure 2C) were observed in the EAE group, with only a trend to significance (P=0.0508) in the case of GFAP and P2X4 receptor. Additionally, the R^2 values for the combination IL-1β and either Iba1 (R^2=0.4070) or GFAP (R^2=0.3505) suggest the existence of a correlation which does not reach statistical significance possibly due to the limited number of replicates. Although preliminary, these data suggest that the mechanisms that drives glial cell activation at early time points can be slightly different from additional mechanisms that contribute to pain maintenance and chronicization over the course of the pathology.

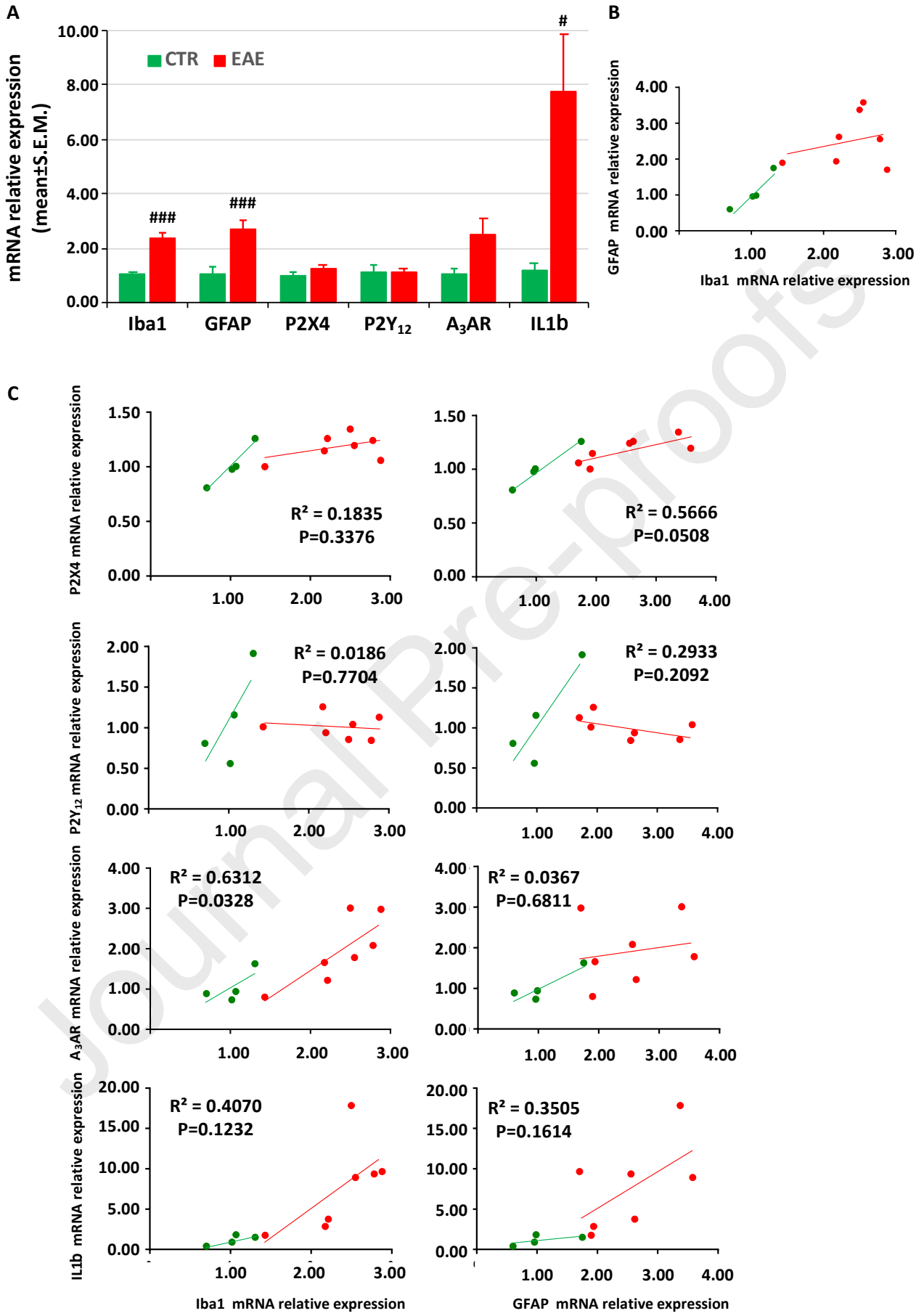

Supplementary Figure 2. Increased expression of glial markers and of IL-1β in the brainstem of EAE animals at the onset of the disease. A: *Real-time qPCR showing mRNA expression of the astrocytic marker GFAP, of the microglia marker Iba1, of IL-1β, of the P2X4 and $P2Y_{12}$ nucleotide receptors and of the A_3 adenosine receptor in the brainstem of EAE animals sacrificed at the onset of the pathology (i.e., the first day in which they showed a clinical score≥1) [37]. CTR animals were sacrificed in parallel. N=4 (CTR) and 8 (EAE) animals from 1 experiment. #P<0.05; ###P<0.001 vs CTR; unpaired, two-tailed Student's t test.* ***B:*** *XY dispersion of samples in the CTR and EAE groups based on the expression of Iba1 (X axis) and GFAP (Y axis).* ***C:*** *XY dispersion of samples in the CTR and EAE groups based on the expression of the glial markers Iba1 or GFAP (X axis) and of the various purinergic receptors or IL-1β (Y axis). Pearson correlations have been calculated for each group separately. The R^2 and P values refer to EAE samples. N=4 (CTR) and 7 (EAE) animals from 1 experiment.*

3.5 Activated satellite glial cells and altered metabolic profile in the TG ganglia of EAE animals at DPI 21

We next moved to the TG system and analyzed the possible activation of TG resident glial cells, i.e. satellite glial cells (SGCs), which are crucially involved in different experimental models of inflammatory and neuropathic orofacial allodynia [11;30]. As shown in Figure 6A, the number of neurons encircled by SGCs expressing GFAP, a marker of their activation [51], was significantly increased in the TG of EAE rats with respect to Naïve and CTR animals (see also representative pictures). We also evaluated the possible TG infiltration of circulating macrophages, an additional sign of TG inflammation and sensitization [51]. A trend to increase in the number of infiltrating Iba1-positive macrophages was detected in tissues from EAE animals (Figure 6B), thus suggesting a possible contribution of this cell type to TG inflammation and sensitization.

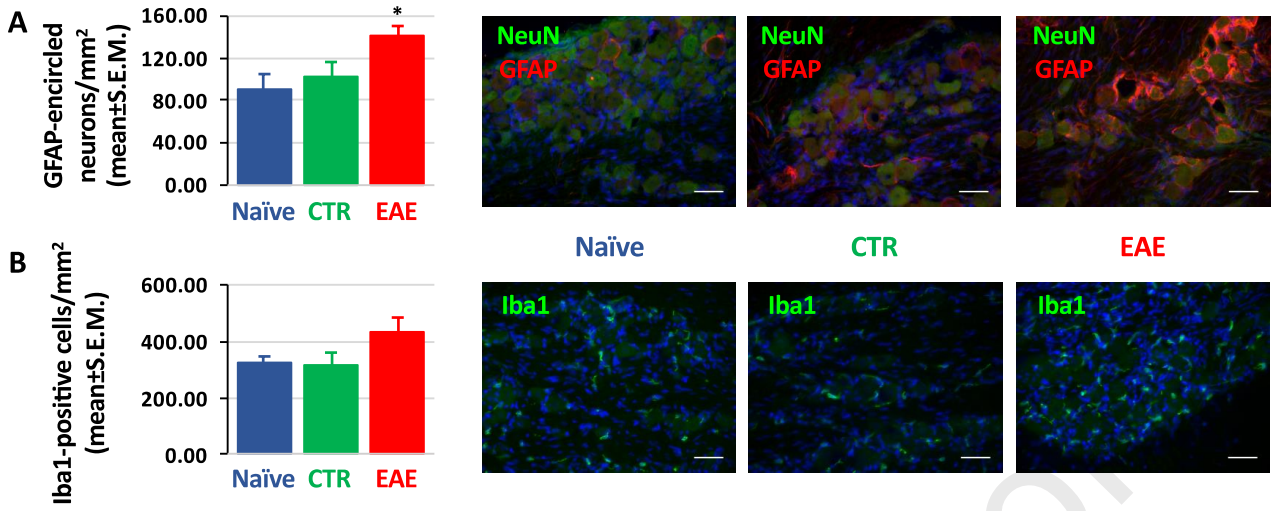

Figure 6. Activation of satellite glial cells in the TG ganglia of EAE animals at DPI 21. A: *TG ganglion sections have been co-stained with anti-NeuN and anti-GFAP antibodies to visualize neurons and activated surrounding satellite glial cells, respectively [30]. The number of GFAP-encircled neurons has been counted in each section and expressed as a function of the area of the tissue in mm^2.* ***B:*** *TG ganglion sections have been stained with anti-Iba1 antibodies to identify infiltrating macrophages. The number of positive cells has been counted in each section and expressed as a function of the area of the tissue in mm^2. N=6 sections from 4 animals/condition. *P<0.05 vs Naïve; one-way ANOVA, Tukey post-hoc test. Representative micrographs for each condition are shown on the right. Nuclei are stained with the Hoechst 33258 dye. Scale bars: 50 µm.*

In the search for signaling molecules directly involved in the development of EAE-induced TG sensitization, we have performed a mass spectrometry-based metabolomic analysis [4] of the TG nerves and ganglia of animals at DPI 21. More than 200 metabolites (including energy metabolites involved in glycolysis, pentose phosphate pathway, TCA cycle, energetic cofactors, amino acids and different classes of phospholipids) have been analyzed. We have applied very stringent limits to the statistical analysis of data (false discovery rate 0.05). Additionally, to rule out any possible interference due to the development of unspecific inflammation in CTR animals (see above), we have focused only on metabolites that were significantly altered in the EAE group with respect to both CTR and Naïve animals (and that were not different between the latter two groups). While no significant changes can be observed in TG nerves (Figure 7A and Supplementary figure 3), about 50 metabolites have been found significantly modified by EAE induction in the TG ganglia (Figure 7B and Supplementary figure 4). They include several phospholipids (Table 2) and, more importantly, a drop in the production of energy metabolites and an increase in amino acids (Table

3), which are likely involved in alterations of the metabolic coupling of nociceptors and activated SGCs within TG.

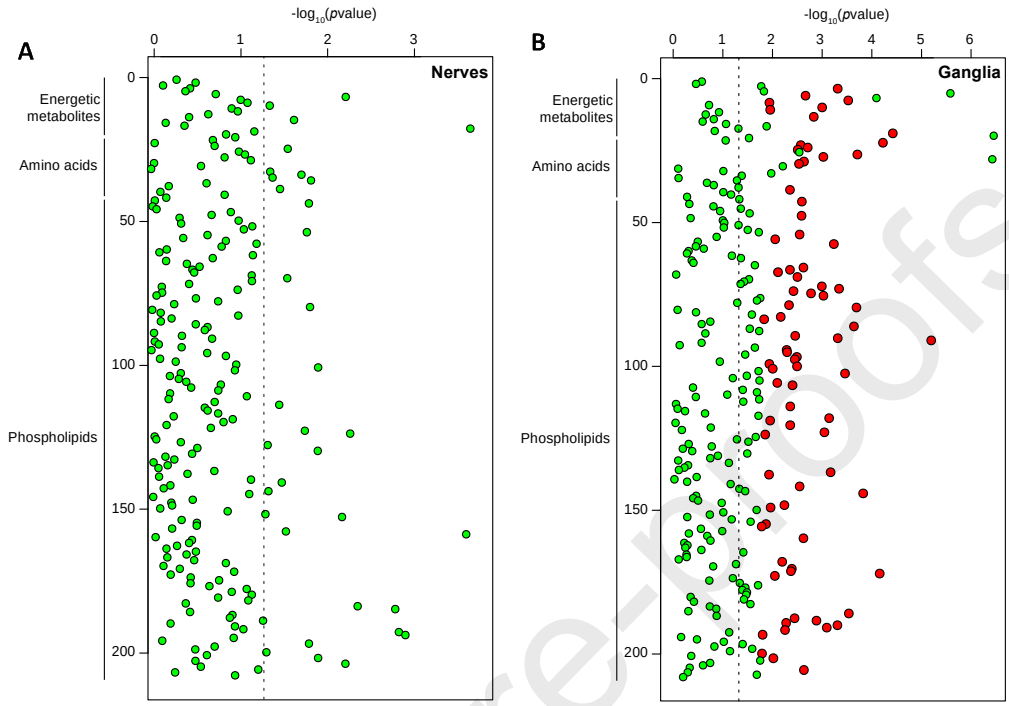

Figure 7. Significant metabolic alterations in the TG ganglia of EAE animals at DPI 21. *Statistical analysis of energetic metabolites (glycolysis, pentose phosphate pathway, TCA cycle, energetic cofactors), amino acids and phospholipids (sphingomyelin, ceramides, lysophosphatidylcholines, phosphatidylcholines, lysophosphatidylethanolamines, phosphatidylethanolamines, plasmalogens, sulfatides, phosphatidylglycerols, lysophosphatidic acids, phosphatidic acids, lysophosphatidylinositols, phosphatidylinositols) in trigeminal nerves* ***(A)*** *and ganglia* ***(B)****.* ***A:*** *N=16 (Naïve), 9 (CTR) and 17 (EAE).* ***B:*** *N=10 (Naïve and EAE) and 8 (CTR). One-Way ANOVA was performed using Fisher's post-hoc test with low standard deviation. Red and green dots represent significant and non-significant values, respectively, between Naïve vs EAE and CTR vs EAE. The lists of significantly altered phospholipids and energetic metabolites are reported in Tables 2 and 3, respectively.*

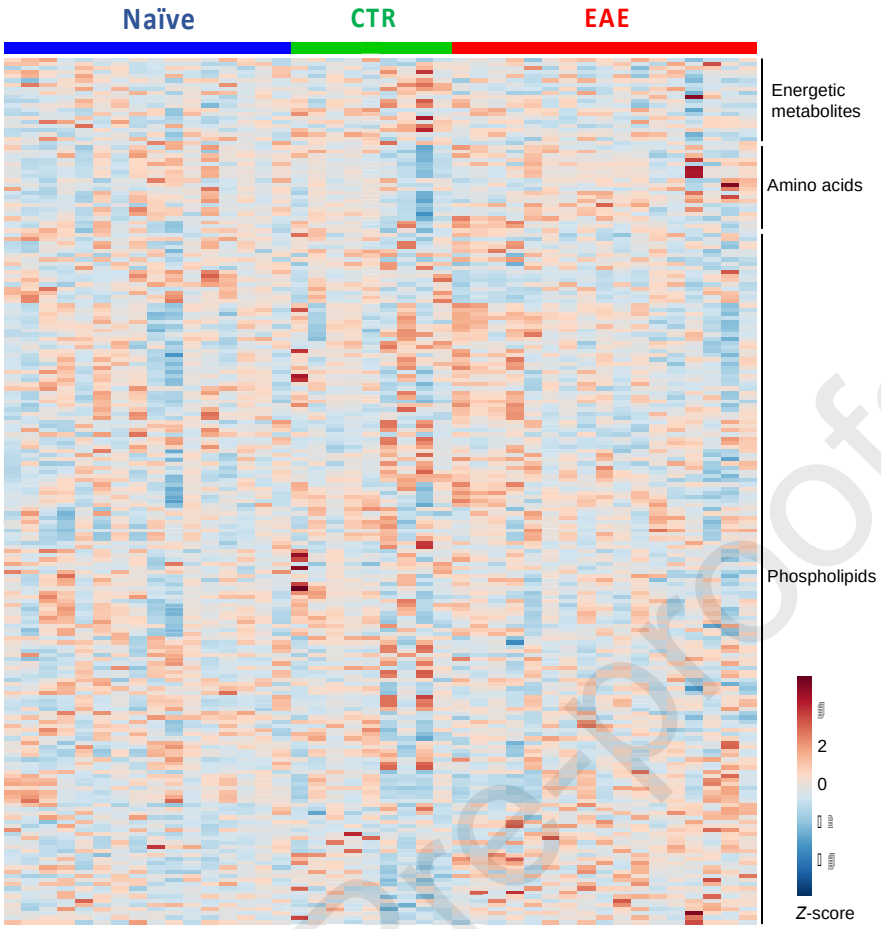

Supplementary figure 3. Metabolomic analysis of the trigeminal nerves from Naïve, CTR and EAE animals at DPI 21. *Heatmap analysis of energetic metabolites (glycolysis, pentose phosphate pathway, TCA cycle, energetic cofactors), amino acids and phospholipids (sphingomyelin, ceramides, lysophosphatidylcholines, phosphatidylcholines, lysophosphatidylethanolamines, phosphatidyl-ethanolamines, plasmalogens, sulfatides, phosphatidylglycerols, lysophosphatidic acids, phosphatidic acids, lysophosphatidylinositols, phosphatidylinositols) in the trigeminal nerves of animals in the different experimental conditions. Each lane represents 1 animal. Heatmap is represented as Z-score calculated for each metabolite. N=16 (Naïve), 9 (CTR) and N=17 (EAE) rats from 3 independent experiments.*

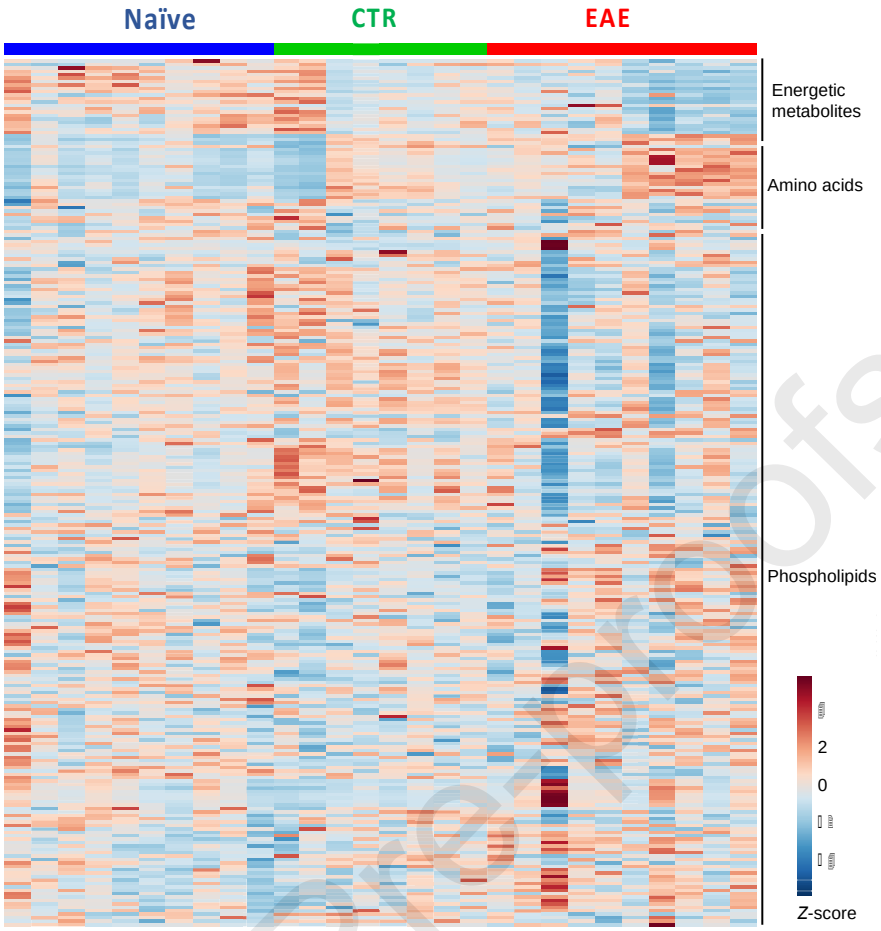

Supplementary figure 4. Metabolomic analysis of the trigeminal ganglia from Naïve, CTR and EAE animals at DPI 21. *Heatmap analysis of energetic metabolites (glycolysis, pentose phosphate pathway, TCA cycle, energetic cofactors), amino acids and phospholipids (sphingomyelin, ceramides, lysophosphatidylcholines, phosphatidylcholines, lysophosphatidylethanolamines, phosphatidyl-ethanolamines, plasmalogens, sulfatides, phosphatidylglycerols, lysophosphatidic acids, phosphatidic acids, lysophosphatidylinositols, phosphatidylinositols) in the trigeminal nerves of animals in the different experimental conditions. Each lane represents 1 animal. Heatmap is represented as Z-score calculated for each metabolite. N=10 (Naïve), 8 (CTR) and 10 (EAE) rats from 3 independent experiments.*

Table 2. Phospholipids significantly modified in Naïve vs EAE and CTR vs EAE groups.

Metabolite	Fold change EAE vs Naïve	Fold change EAE vs Ctr	-$\log_{10}$ *p*value	FDR
lyso PA C18:1	0.81	0.79	1.78	0.049
lyso PC C18:0	0.78	0.74	2.03	0.033

lyso PC C18:2	0.70	0.70	2.52	0.018
lyso PC C20:3	0.70	0.77	3.21	0.008
PA C32:1	1.29	1.41	3.51	0.006
PA C34:1	1.71	1.50	2.86	0.012
PA C34:2	1.39	1.33	2.42	0.019
PA C36:1	1.35	1.33	3.28	0.007
PA C36:2	1.27	1.18	2.25	0.023
PA C38:4	1.40	1.45	3.07	0.009
PC aa C32:2	0.86	0.82	2.33	0.020
PC aa C32:3	0.70	0.73	2.60	0.017
PC aa C34:4	0.74	0.74	2.48	0.018
PC aa C36:2	0.87	0.80	3.00	0.010
PC aa C36:3	0.86	0.78	2.75	0.014
PC aa C36:4	0.91	0.84	2.40	0.019
PC aa C36:5	0.71	0.76	3.32	0.007
PC aa C36:6	0.71	0.80	2.97	0.010
PC aa C38:4	0.82	0.73	3.67	0.005
PC aa C38:5	0.88	0.82	2.31	0.021
PC aa C40:1	1.22	1.39	3.62	0.005
PC aa C42:1	1.31	1.58	3.29	0.007
PC aa C42:2	1.22	1.32	2.44	0.019
PE aa C32:0	1.36	1.28	1.93	0.038
PE aa C32:1	1.30	1.35	3.12	0.009
PE aa C34:2	1.21	1.26	3.02	0.010

PE aa C40:2	1.36	1.50	2.52	0.018
PE aa C42:4	1.15	1.30	2.22	0.024
PE aa C44:0	0.76	0.82	1.85	0.044
PE ae C42:0	0.85	0.84	2.03	0.033
PE ae C42:1	0.77	0.83	4.14	0.003
PI C36:1	1.67	2.43	1.77	0.049
PI C38:4	1.38	1.54	1.99	0.035
SM C20:2	0.70	0.74	2.33	0.020

False Discovery rate (FDR) <0.05.

Lyso PA, lysophosphatidic acid; LysoPC, lysophosphatidylcholine; PA, phosphatidic acid; PCaa, phosphatidylcholine acyl-acyl; PEaa, phosphatidylethanolamine acyl-acyl; PCae, phosphatidylcholine acyl-alkyl; PI, phosphatidylinositol; SM, sphingomyelin. C represents the number of total fatty acids bound to a given phospholipid while the number after colons represent the total number of insaturation of fatty bound to a given phospholipid.

Note: Phospholipid molecules characterized by the presence of a vinyl ether linkage at the sn-1 position and an ester linkage at the sn-2 position of the glycerol moiety (alkyl-acyl form, ae) are known as plasmalogens.The most common plasmalogens in mammals carries either ethanolamine (plasmenylethalomines) or choline (plasmenylcholines) as head group. The PC aa and PE aa phospholipids carries fatty acids as ester linkage at both sn-1 and sn-2 positions (acyl-acyl form, aa).

Table 3. Energetic metabolites significantly modified in Naïve vs EAE and CTR vs EAE groups.

Metabolite	Fold change EAE vs Naïve	Fold change EAE vs Ctr	-$\log_{10}$ *p*value	FDR
Lactate	0.62	0.71	3.29	0.017
Acetyl-CoA	0.65	0.72	2.64	0.006
α-Ketoglutarate	0.59	0.64	3.50	0.018
Fumarate	0.62	0.66	2.98	0.005

Malate	0.71	0.72	1.93	0.013
NADH	0.61	0.63	1.86	0.010
ATP	0.63	0.65	2.81	0.010
Aspargine	2.10	1.74	2.52	0.002
Aspartate	1.84	1.52	3.69	0.018
Glutamine	1.89	1.83	3.01	0.018
Glycine	1.97	1.45	4.40	0.007
Histidine	2.13	1.54	2.51	0.016
Isoleucine	2.08	1.68	2.48	0.038
Leucine	2.01	1.70	2.69	0.043
Threonine	1.83	1.46	2.55	0.018
Valine	2.00	1.51	4.20	0.003

False Discovery rate (FDR) <0.05.

Discussion

Our main findings are: i) the demonstration of the spontaneous development of trigeminal pain in a rat model of relapsing-remitting EAE in the absence of brainstem demyelination and before the motor onset of the pathology; ii) the presence of activated glial cells in the brainstem paralleled by the upregulation of purinergic receptors; iii) the identification of reactive glial cells and of an altered metabolic and phospholipid profile in the TG ganglion of EAE animals, with no alterations in the TG nerves.

Another important issue emerging from our data is the inclusion of a vehicle-injected CTR group. The development of unspecific paw swelling and inflammation leading to decreased head withdrawal threshold was unexpected but allowed us to demonstrate that extremely specific changes in glia cell activation, metabolic impairments etc. (see above) can be only detected following induction of EAE. Thus, based on our data it is mandatory to include both Naïve and CTR animals in any experimental plan.

Based on the high prevalence of TG pain and migraine even before the first diagnosis of MS in patients, the identification of both central and peripheral sites of molecular and cellular alterations (Supplementary figure 5) opens the way towards targeted pharmacological approaches to slow down and relieve pain development.

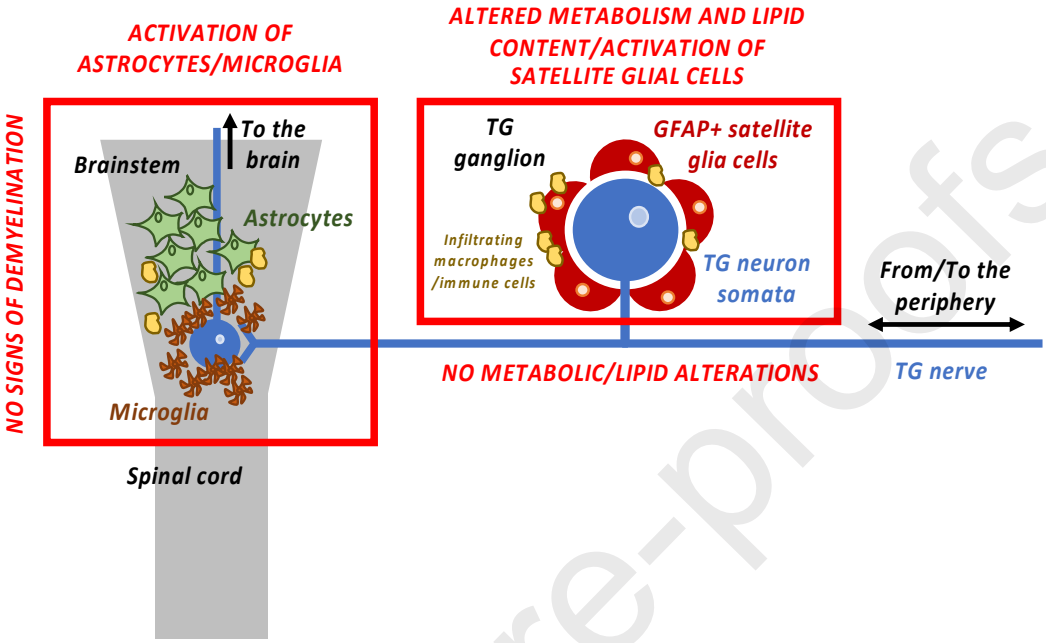

Supplementary figure 5. Schematic representation of our results at DPI 21. *Metabolic dysregulation in the TG ganglion, accompanied by satellite glial cells activation, and astrogliosis/microgliosis in the brainstem have been identified in EAE animals at DPI 21. The lack of metabolic/lipid alterations in the TG nerve and the absence of signs of brainstem demyelination suggest that the actual driver of TG sensitization should be identified in one of the two above-mentioned sites, with TG nerve only behaving as a "connecting railroad" for pathologic signals. See text for details.*

Relapsing-remitting MS is the most diffuse type of MS among young adults [53], and therefore the analysis of pain development in rodent models of EAE showing peaks and remission of motor symptoms allows a future translation to human pathology. The development of hind paw sensitization, as a marker of neuropathic pain, has been already demonstrated in mice [21;22], and in Dark Agouti rats [16;44] exposed to relapsing-remitting EAE (the latter being the animal model utilized in the present study). Concerning TG pain, few previous papers analyzed its development in mouse models of chronic progressive EAE [12;13;50], but to date no results have been published in relapsing-remitting EAE. We observed TG sensitization well before EAE onset, with a constant reduction of the head withdrawal threshold independently from the disease stage and no recovery

during remission. This parallels the observation of an early insurgence of hind paw mechanical and thermal hyperalgesia in rats [49] and of mechanical allodynia in mice [13] exposed to chronic EAE, and reminds the human condition with no clear correlation between the disease stage and the severity of episodes of TG pain [34].

As mentioned, whether TG sensitization in MS is a direct consequence of central demyelination or not is still a matter of debate. Pre-clinical and clinical data sustain either of the two hypotheses [26]. Our functional data show a clear discrepancy between the onset of TG pain and of relapsing-remitting EAE motor disturbances thus supporting the notion of two parallel pathways. This seems to be a typical feature of TG sensitization independently from the overall course of EAE, since orofacial allodynia develops at the onset [50] or well before [12;13] the appearance of motor signs of chronic EAE in mice as well. Our data are supported by the lack of alterations in brainstem myelin. In the case of demyelinating plaques, gross changes in myelin staining and a significant reduction in the expression of MBP and CNPase are detected [9], which do not occur in our experimental model.

Activation of glial cells in the CNS is a hallmark of both chronic pain and of neurodegenerative disorders. Following peripheral nerve damage, spinal cord microglia sense a variety of neuron-derived stimuli, leading to their transition towards a reactive state which represents one fundamental driver of neuronal sensitization and pain chronicization [15]. Microglia activation is followed by immune cell recruitment and by the appearance of neurotoxic A1 astrocyte subpopulation [23]. Altogether, this complex cell-to-cell communication contributes to generate a highly pro-inflammatory milieu, whose effects can extend for months after the initial nerve damage and guide the transition from acute to chronic neuropathic pain [43].

CNS glial cells are also directly implicated in EAE pathophysiology. Astrocytes suffer cell damage at early time points leading to the disruption of the blood-brain barrier and are the main sources of chemokines thus contributing to neuroinflammation, but they also constitute a protective barrier towards the excessive infiltration of immune cells from the periphery [3]. Activated microglia also contribute to neurodegeneration in EAE progression, and opposite detrimental [54] or beneficial effects [56] have been described. Based on the known double-edged sword nature of reactive glia, it is impossible to foresee the final functional outcome only based on their activated morphology, since it possibly depends on the pro/anti-inflammatory phenotype of cells, on their tissue location (e.g., pro-inflammatory microglia phagocyte and clear toxic myelin debris close to demyelinating plaques) and on the disease stage.

Our data showing activation of glial cells in the brainstem of EAE animals at 21 DPI, but also at the onset of the pathology when TG sensitization is already manifested, suggest a role for these cells in the development of EAE-associated symptoms and their potential as targets for innovative pharmacological interventions. We have identified glial receptors whose pro-algogenic role has been already demonstrated in different types of pain but never evaluated in EAE-related TG sensitization. Ionotropic P2X4 receptors (P2X4Rs) have been long known as key triggers of microglia activation following injury and in painful conditions. Specifically, their inhibition reduces cell activation and neuropathic pain in male but not in female rodents [17;32], suggesting the existence of a sexual dimorphism in the mechanisms driving the development of pain. A specific role has been also demonstrated in male animals exposed to nitroglycerin-induced migraine [25], but no data are available in EAE-related TG pain. Thus, despite the higher prevalence of both MS [31] and TG pain [41] in females, preclinical data highlight the importance of analyzing male animals as well to identify relevant targets for both sexes.

Also $P2Y_{12}$ receptors ($P2Y_{12}Rs$) have been involved in the activation of microglia and in the development of pain with a predominant pro-algogenic role [55]. At variance from the almost exclusive microglia localization of P2X4Rs, $P2Y_{12}Rs$ are also expressed by platelets and T cells [36] and are the targets of blockbuster thienopyridine anti-platelet drugs. Interestingly, both P2X4Rs and $P2Y_{12}Rs$ are upregulated along the course of EAE [10]. While antagonists of the latter receptor subtype are able to slow down the motor signs of the disease by acting on T cells in the periphery [36], the P2X4R should be activated by agonists to get a positive response of microglia cells against the infiltration of autoreactive T cells [56]. Thus, whether an agonist or an antagonist could prove beneficial for both disease progression and associated pain development must be clearly addressed.

Finally, the A_3 adenosine receptor subtype (A_3AR) shows a prevalent glial expression and selective agonists have proven analgesic and anti-allodynic in various rodent models of neuropathic pain [20;24], also through the inhibition of microglia activation [48]. Its trend for upregulation in the brainstem of rats at the onset of EAE suggests that it may represent the most interesting pharmacological target for an early therapeutic approach to EAE-induced TG pain. Future studies are needed to clearly identify the triggers of activation for brainstem astrocytes and microglia in EAE rats since our preliminary data at the onset of the pathology suggest the possible existence of early events (i.e., the recruitment of A_3ARs) which are later followed and sustained by additional mechanisms involving P2 receptors.

Concerning satellite glial cells (SGCs) which reside in sensory ganglia, several papers already demonstrated that their activation can promote neuronal sensitization and pain, not only at the level of the TG ganglion but also in DRGs [30;46;51]. One single paper has demonstrated activation of DRG SGCs 10 days after the induction of progressive EAE in mice, in parallel with the development of hind paw neuropathic pain [52]. To the best of our knowledge, our data are the first demonstration of SGCs reaction in the TG ganglia during the development of EAE-related TG pain, along with metabolic and lipid alterations. Published data looking for a link between metabolic alterations and neuropathic pain have mostly focused on diabetes and have overall detected no alterations in sensory ganglia but rather metabolic changes in the sciatic and sural nerves, which are directly related to the development of peripheral neuropathy and pain [4;18]. Pathological changes in CNS neuron-glia "metabolic coupling" have been demonstrated in several models of neurodegeneration and neuropathic pain [38]. In our experimental model, the lack of significant metabolic modifications in the TG nerves of EAE animals suggests that, besides CNS sensitization and glia activation, an additional possible trigger for the development of TG sensitization is represented by the altered metabolic support between activated SGCs and sensory TG neurons. From a metabolic point of view, our data show that EAE induces a metabolic rewiring consisting in the reduction of lactate and metabolites belonging to tricarboxylic acid (TCA) cycle. All of this seems to sustain anaplerotic reactions to generate amino acids (several are found increased in ganglia) to the detriment of NADH and ATP levels. In other words, TCA cycle intermediates do not properly flux in the cycle to sustain NADH levels and energy production (in the form of ATP) but are diverted toward amino acid synthesis. Impaired energy production is paralleled by a significant reduction in the levels of fumarate in the TG ganglia of EAE animals. Dimethyl-fumarate (DMF) is a recently approved disease-modifying drug for MS, whose yet-to-be fully clarified mechanism of action involves the activation of the hydroxycarboxylic acid receptor type 2 (HCAR2) [7]. Interestingly, both DMF and the endogenous agonist of HCAR2, the ketone body β-hydroxybutyrate (BHB), exert antiallodynic actions in rodent models of neuropathic pain [2] also through the inhibition of microglia activation [35]. Thus, it is tempting to speculate that EAE-induced alterations of HCAR2 signaling pathway could contribute to the development of TG pain, and that administration of DMF or of a ketogenic diet, which increases BHB levels, could be of help.

With this paper we aimed at setting up the EAE model in rats and at analyzing changes at DPI 21. We are aware of the fact that the main drawback of our data is represented by the lack of a full characterization of the observed alterations at the onset of EAE and of EAE-related TG pain. This will

be the focus of our future work. A main point to be understood is whether early TG metabolic alterations occur which translate into activation of CNS glial cells or the opposite way around. Additionally, no published data are available on the modulation of cell metabolism by purinergic receptors; in this respect, the analysis of brainstem metabolism would help clarifying the mechanisms that trigger TG sensitization in EAE. Nevertheless, our preliminary results suggest that microglia and astrocytes are already activated at the onset of EAE and release pro-inflammatory IL-1β, in parallel with a trend for the upregulation of A_3ARs. These are the bases to start with the identification of the actual trigger of TG sensitization following induction of EAE, and of new pharmacological targets for the development of innovative painkillers. To date, in fact, available pharmacological approaches to EAE-related TG neuralgia are often unsatisfactory, and bear significant side effects (e.g., in the case of antiepileptics), leading to comorbidities, such as depression, anxiety and fatigue [45].

Acknowledgements

This work was supported by: FISM–Fondazione Italiana Sclerosi Multipla (grant #2016/R/7 to SC); Università degli Studi di Milano-Piano di Sostegno alla Ricerca 2017 Linea 2 (to SC); Italian Ministry of Research (MIUR) Finanziamento Annuale Individuale delle Attività di Base di Ricerca 2017 (to SC); Università degli Studi di Milano-Intramural Transition Grant (to NM); MIUR "Department of Excellence" grant program to the Department of Pharmacological and Biomolecular Sciences. Authors are grateful to Dr. Laura Madaschi (UniTech NOLIMITS facility, Università degli Studi di Milano) for her precious help in collecting images of brainstem sections. Authors declare no conflict of interest.

References

[1] Audano M, Pedretti S, Crestani M, Caruso D, De Fabiani E, Mitro N. Mitochondrial dysfunction increases fatty acid β-oxidation and translates into impaired neuroblast maturation. FEBS Lett. 2019; 593(22):3173–89.

[2] Boccella S, Guida F, De Logu F , De Gregorio D, Mazzitelli M, Belardo C, Iannotta M, Serra N, Nassini R, de Novellis V, Geppetti P, Maione S, Luongo L. Ketones and Pain: Unexplored Role of Hydroxyl Carboxylic Acid Receptor Type 2 in the Pathophysiology of Neuropathic Pain. FASEB J. 2019; 33(1):1062-73.

[3] Brambilla R. The contribution of astrocytes to the neuroinflammatory response in multiple sclerosis and experimental autoimmune encephalomyelitis. Acta Neuropathologica 2019; 137:757–83.

[4] Cermenati G, Audano M, Giatti S, Carozzi V, Porretta-Serapiglia C, Pettinato E, Ferri C, D'Antonio M, De Fabiani E, Crestani M, Scurati S, Saez E, Azcoitia I, Cavaletti G, Garcia-Segura LM, Melcangi RC, Caruso D, Mitro N. Lack of sterol regulatory element binding factor-1c imposes glial Fatty Acid utilization leading to peripheral neuropathy. Cell Metab 2015; 21(4):571-83

[5] Cermenati G, Giatti S, Audano M, Pesaresi M, Spezzano R, Caruso D, Mitro N, Melcangi RC. Diabetes alters myelin lipid profile in rat cerebral cortex: Protective effects of dihydroprogesterone. J Steroid Biochem Mol Biol. 2017; 168:60–70.

[6] Ceruti S. What role does multiple sclerosis play in the development of untreatable painful conditions? Pain Manag 2018; 8(1):37-44

[7] Chen H, Assmann JC, Krenz A, Rahman M, Grimm M, Karsten CM, K¨ohl J, Offermanns S, Wettschureck N, Schwaninger M. Hydroxycarboxylic acid receptor 2 mediates dimethylfumarate's protective effect in EAE. J Clin Invest. 2014; 124:2188–92

[8] Chong J, Wishart DS, Xia J. Using MetaboAnalyst 4.0 for Comprehensive and Integrative Metabolomics Data Analysis. Curr Protoc Bioinformatics 2019; 68(1):e86

[9] Coppolino GT, Marangon D, Negri C, Menichetti G, Fumagalli M, Gelosa P, Dimou L, Furlan R, Lecca D, Abbracchio MP. Differential local tissue permissiveness influences the final fate of GPR17-expressing oligodendrocyte precursors in two distinct models of demyelination. Glia 2018; 66(5):1118-30

[10] Domercq M, Zabala A, Matute C. Purinergic Receptors in Multiple Sclerosis Pathogenesis. Brain Res Bull 2019; 151:38-45.

[11] Donegan M, Kernisant M, Cua C, Jasmin L, Ohara PT. Satellite glial cell proliferation in the trigeminal ganglia after chronic constriction injury of the infraorbital nerve. Glia 2013; 61(12):2000-8.

[12] Duffy SS, Keating BA, Perera CJ, Lees JG, Tonkin RS, Makker PGS, Carrive P, Butovsky O, Moalem-Taylor G. Regulatory T Cells and Their Derived Cytokine, Interleukin-35, Reduce Pain in Experimental Autoimmune Encephalomyelitis. J Neurosci 2019; 39(12):2326-46

[13] Duffy SS, Perera CJ, Makker PG, Lees JG, Carrive P, Moalem-Taylor G. Peripheral and Central Neuroinflammatory Changes and Pain Behaviors in an Animal Model of Multiple Sclerosis. Front Immunol 2016; 7:369

[14] Ferroli P, Farina L, Franzini A, Milanese C, Broggi G. Linear pontine and trigeminal root lesions and trigeminal neuralgia. Arch Neurol 2001; 58(8):1311-2

[15] Grace PM, Hutchinson MR, Maier SF, Watkins LR. Pathological pain and the neuroimmune interface. Nat Rev Immunol 2014; 14(4):217-31

[16] Grace PM, Loram LC, Christianson JP, Strand KA, Flyer-Adams JG, Penzkover KR, Forsayeth JR, van Dam A-M, Mahoney MJ, Maier SF, Chavez RA, Watkins LR. Behavioral Assessment of

Neuropathic Pain, Fatigue, and Anxiety in Experimental Autoimmune Encephalomyelitis (EAE) and Attenuation by interleukin-10 Gene Therapy. Brain Behav Immun 2017; 59:49-54.

[17] Halievski K, Ghazisaeidi S, Salter MW. Sex-dependent mechanisms of chronic pain: A focus on microglia and P2X4R .J Pharmacol Exp Ther. 2020; doi: 10.1124/jpet.120.265017. Online ahead of print.

[18] Hinder LM, Vivekanandan-Giri A, McLean LL, Pennathur S, Feldman EL. Decreased Glycolytic and Tricarboxylic Acid Cycle Intermediates Coincide With Peripheral Nervous System Oxidative Stress in a Murine Model of Type 2 Diabetes. J Endocrinol 2013; 216(1):1-11.

[19] Husain F, Pardo G, Rabadi M. Headache and Its Management in Patients With Multiple Sclerosis. Curr Treat Options Neurol 2018; 20(4):10

[20] Janes K, Symons-Liguori AM, Jacobson KA, Salvemini D. Identification of A_3 adenosine receptor agonists as novel non-narcotic analgesics. Br J Pharmacol. 2016; 173:1253-67.

[21] Khan N, Gordon R, Woodruff TM, Smith MT. Antiallodynic effects of alpha lipoic acid in an optimized RR-EAE mouse model of MS-neuropathic pain are accompanied by attenuation of upregulated BDNF-TrkB-ERK signaling in the dorsal horn of the spinal cord. Pharmacol Res Perspect. 2015; 3(3):e00137.

[22] Khan N, Woodruff TM, Smith MT. Establishment and characterization of an optimized mouse model of multiple sclerosis-induced neuropathic pain using behavioral, pharmacologic, histologic and immunohistochemical methods. Pharmacol Biochem Behav. 2014; 126:13-27.

[23] Liddelow SA, Guttenplan KA, Clarke LE, Bennett FC, Bohlen CJ, Schirmer L, Bennett ML, Münch AE, Chung W-S, Peterson TC, Wilton DK, Frouin A, Napier BA, Panicker N, Kumar M, Buckwalter MS, Rowitch DH, Dawson VL, Dawson TM, Stevens B, Barres BA. Neurotoxic Reactive Astrocytes Are Induced by Activated Microglia. Nature 2017; 541(7638):481-7

[24] Little JW, Ford A, Symons-Liguori AM, Chen Z, Janes K, Doyle T, Xie J, Luongo L, Tosh DK, Maione S, Bannister K, Dickenson AH, Vanderah TW, Porreca F, Jacobson KA, Salvemini D. Endogenous Adenosine A_3 Receptor Activation Selectively Alleviates Persistent Pain States. Brain 2015; 138:28-35

[25] Long T, He W, Pan Q , Zhang S, Zhang D, Qin G, Chen L, Zhou J. Microglia P2X4R-BDNF Signalling Contributes to Central Sensitization in a Recurrent Nitroglycerin-Induced Chronic Migraine Model. J Headache Pain 2020; 21(1):4.

[26] Maarbjerg S, Di Stefano G, Bendtsen L, Cruccu G. Trigeminal Neuralgia - Diagnosis and Treatment. Cephalalgia 2017, 37(7):648-57

[27] Magni G, Boccazzi M, Bodini A, Abbracchio MP, van den Maagdenberg AM, Ceruti S. Basal astrocyte and microglia activation in the central nervous system of Familial Hemiplegic Migraine Type I mice. Cephalalgia 2019; 39(14):1809-1817.

[28] Magni G, Ceruti S. The role of adenosine and P2Y receptors expressed by multiple cell types in pain transmission. Brain Res Bull 2019; 151:132-43.

[29] Magni G, Marinelli A, Riccio D, Lecca D, Tonelli C, Abbracchio MP, Petroni K, Ceruti S. Purple Corn Extract as Anti-allodynic Treatment for Trigeminal Pain: Role of Microglia. Front Cell Neurosci 2018; 12:378.

[30] Magni G, Merli D, Verderio C, Abbracchio MP, Ceruti S. $P2Y_2$ receptor antagonists as anti-allodynic agents in acute and sub-chronic trigeminal sensitization: Role of satellite glial cells. Glia 2015; 63(7):1256-69.

[31] Magyari M, Sorensen PS. The changing course of multiple sclerosis: rising incidence, change in geographic distribution, disease course, and prognosis. Curr Opin Neurol. 2019; 32(3):320-6.

[32] Mapplebeck JCS, Dalgarno R, Tu Y, Moriarty O, Beggs S, Kwok CHT, Halievski K, Assi S, Mogil JS, Trang T and Salter MW. Microglial P2X4R-evoked pain hypersensitivity is sexually dimorphic in rats. Pain 2018; 159(9):1752-63.

[33] Massier J, Eitner A, von Banchet GS, Schaible HG. Effects of differently activated rodent macrophages on sensory neurons. Implications for arthritic pain. Arthritis Rheumatol 2015; 67:2263-72

[34] O'Connor AB, Schwid SR, Herrmann DN, Markman JD, Dworkin RH. Pain associated with multiple sclerosis: systematic review and proposed classification. Pain 2008; 137(1):96-111.

[35] Qian J, Zhu W, Lu M, Ni B, Yang J. Dβ-hydroxybutyrate promotes functional recovery and relieves pain hypersensitivity in mice with spinal cord injury. Br J Pharmacol. 2017; 174:1961–71.

[36] Qin C, Zhou J, Gao Y, Lai W, Yang C, Cai Y, Chen S and Du C. Critical Role of $P2Y_{12}$ Receptor in Regulation of Th17 Differentiation and Experimental Autoimmune Encephalomyelitis Pathogenesis. J Immunol 2017; 199(1):72-81.

[37] Ramos KM, Lewis MT, Morgan KN, Crysdale NY, Kroll JL, Taylor FR, Harrison JA, Sloane EM, Maier SF, Watkins LR. Spinal upregulation of glutamate transporter GLT-1 by ceftriaxone: therapeutic efficacy in a range of experimental nervous system disorders. Neuroscience 2010; 169(4):1888-900

[38] Robinson RR, Dietz AK, Maroof AM, Asmis R, Forsthuber TG. The role of glial-neuronal metabolic cooperation in modulating progression of multiple sclerosis and neuropathic pain. Immunotherapy 2019; 11(2):129-47

[39] Schindelin J, Arganda-Carreras I, Frise E, Kaynig V, Longair M, Pietzsch T, Preibisch S, Rueden C, Saalfeld S, Schmid B, Tinevez JY, White DJ, Hartenstein V, Eliceiri K, Tomancak P, Cardona A. Fiji: an open-source platform for biological-image analysis. Nat Methods 2012; 9(7):676-82

[40] Schneider CA, Rasband WS and Eliceiri KW. NIH Image to ImageJ: 25 years of image analysis. Nature Meth 2012; 9:671-5.

[41] Shaefer JR, Khawaja SN, Bavia PF. Sex, Gender, and Orofacial Pain. Dent Clin North Am. 2018; 62(4):665-82.

[42] Shinoda M, Kubo A, Hayashi Y, Iwata K. Peripheral and Central Mechanisms of Persistent Orofacial Pain. Front Neurosci. 2019;13:1227.

[43] Skaper SD, Facci L, Zusso M, Giusti P. An Inflammation-Centric View of Neurological Disease: Beyond the Neuron. Front Cell Neurosci. 2018; 12:72.

[44] Sloane E, Ledeboer A, Seibert W, Coats B, van Strien M, Maier SF, Johnson KW, Chavez R, Watkins LR, Leinwand L, Milligan ED, Van Dam AM. Anti-inflammatory Cytokine Gene Therapy Decreases Sensory and Motor Dysfunction in Experimental Multiple Sclerosis: MOG-EAE Behavioral and Anatomical Symptom Treatment With Cytokine Gene Therapy. Brain Behav Immun 2009; 23(1):92-100.

[45] Solaro C, Uccelli MM. Management of pain in multiple sclerosis: a pharmacological approach. Nat Rev Neurol 2011; 7(9):519-27

[46] Spray DC, Hanani M. Gap junctions, pannexins and pain. Neurosci Lett 2019; 695:46-52

[47] Swinnen C, Lunskens S, Deryck O, Casselman J, Vanopdenbosch L. MRI characteristics of trigeminal nerve involvement in patients with multiple sclerosis. Mult Scler Relat Disord 2013; 2(3):200-3

[48] Terayama R, Tabata M, Maruhama K, Iida S. A_3 adenosine receptor agonist attenuates neuropathic pain by suppressing activation of microglia and convergence of nociceptive inputs in the spinal dorsal horn. Exp Brain Res 2018; 236:3203–13

[49] Thibault K, Calvino B, Pezet S. Characterisation of sensory abnormalities observed in an animal model of multiple sclerosis: a behavioural and pharmacological study. Eur J Pain. 2011; 15(3):231.e1-16.

[50] Thorburn KC, Paylor JW, Webber CA, Winship IR, Kerr BJ. Facial hypersensitivity and trigeminal pathology in mice with experimental autoimmune encephalomyelitis. Pain 2016; 157(3):627-42

[51] Villa G, Ceruti S, Zanardelli M, Magni G, Jasmin L, Ohara PT, Abbracchio MP. Temporomandibular joint inflammation activates glial and immune cells in both the trigeminal ganglia and in the spinal trigeminal nucleus. Mol Pain 2010; 6:89

[52] Warwick R, Ledgerwood CJ, Brenner T, Hanani M. Satellite Glial Cells in Dorsal Root Ganglia Are Activated in Experimental Autoimmune Encephalomyelitis. Neurosci Lett. 2014; 569:59-62

[53] Yamasaki R, Kira JI. Multiple Sclerosis. Adv Exp Med Biol. 2019; 1190:217-47

[54] Yamasaki R, Lu H, Butovsky O, Ohno N, Rietsch AM, Cialic R, Wu PM, Doykan CE, Lin J, Cotleur AC, Kidd G, Zorlu MM, Sun N, Hu W, Liu L, Lee JC, Taylor SE, Uehlein L, Dixon D, Gu J, Floruta CM, Zhu M, Charo IF, Weiner HL and Ransohoff RM. Differential roles of microglia and monocytes in the inflamed central nervous system. J Exp Med 2014; 211:1533-49.

[55] Yu T, Zhang X, Shi H, Tian J, Sun L, Hu X, Cui W and Du D. $P2Y_{12}$ regulates microglia activation and excitatory synaptic transmission in spinal lamina II neurons during neuropathic pain in rodents. Cell Death Dis. 2019; 10(3):165.

[56] Zabala A, Vazquez-Villoldo N, Rissiek B, Gejo J, Martin A, Palomino A, Perez-Samartín A, Pulagam KR, Lukowiak M, Capetillo-Zarate E, Llop J, Magnus T, Koch-Nolte F, Rassendren F, Matute C, Domercq M. P2X4 Receptor Controls Microglia Activation and Favors Remyelination in Autoimmune Encephalitis. EMBO Mol Med. 2018; 10(8):e8743

[57] Zhu Z, You W, Xie Z, Wang P, Liu Z, Wang C, Bi J. Mycophenolate mofetil improves neurological function and alters blood T-lymphocyte subsets in rats with experimental autoimmune encephalomyelitis. J Int Med Res 2014; 42(2):530-41

HIGHLIGHTS

- Relapsing-remitting EAE in rats is preceded by trigeminal sensitization
- No signs of brainstem demyelination are detected
- Brainstem astrocytes and microglia are activated and upregulate purinergic receptors
- Altered metabolic profile and glia activation in the trigeminal ganglion